Platte River Recovery Implementation Program (PRRIP)

DRAFT

SYSTEM-SCALE GEOMORPHOLOGY AND VEGETATION MONITORING REPORT

2017 - 2020

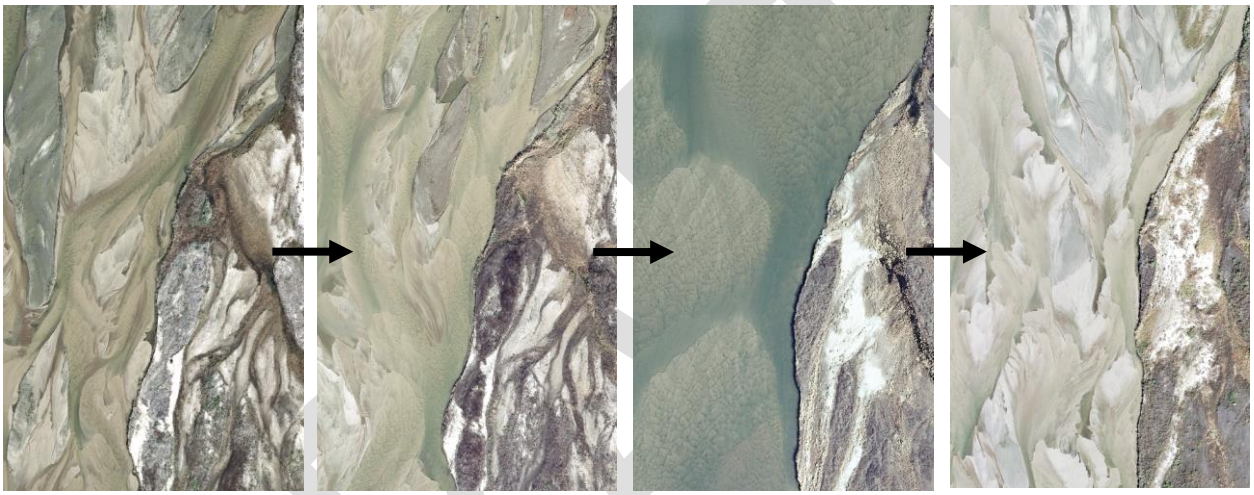

Prepared for: PRRIP Technical Advisory and Governance Committees
Date: 5/5/2022

Prepared By
Executive Director's Office
Platte River Recovery Implementation Program
4111 4th Avenue, Suite 6
Kearney, NE 68845

Suggested Citation:
Executive Director's Office. 2022. Platte River Recovery Implementation Program: 2021 System-Scale Geomorphology and Vegetation Monitoring Report 2017-2020.

Executive Summary

This report documents the first implementation of the PRRIP System-Scale Geomorphology and Vegetation Monitoring effort utilizing remote sensing methods. The goal of the project is to track long-term trends in morphology and in-channel vegetation in the Associated Habitat Reach (AHR) of the Central Platte River, with a focus on changes that may affect habitat for the PRRIP target species. A variety of metrics associated with target species habitat are presented in this report, including trends in wetted width and depth of the channel, width of channel that is unobstructed by tall vegetation, sediment volume differencing, and channel area suitable for whooping crane roosting. Aerial imagery and topobathymetric LiDAR data from annual flights over the Central Platte are analyzed to estimate these metrics. Additionally, data are presented concerning the primary factors that drive habitat change—hydrology and management. This report includes simple comparisons of mean habitat metric values of channel areas managed by PRRIP and other conservation groups vs. unmanaged channel, which allows for a preliminary assessment of the impact of in-channel management. The data may be used in the future to address PRRIP Big Questions, including those concerning the impact of sediment augmentation and germination suppression flow releases on channel conditions. All analyses in this report generally indicate that the AHR remained relatively stable from 2017-2020, with no dramatic shift in channel conditions, despite minor impacts from the 2019 high flow events.

Table of Contents

1. Introduction

The Platte River Recovery Implementation Program (PRRIP or Program) is responsible for implementing aspects of the recovery plan for the endangered whooping crane (*Grus americana*). The Program's Adaptive Management Plan (AMP) management objective is to contribute to the survival of whooping cranes (WC) during migration. Performance indicators include increasing the area of suitable WC roosting and foraging habitat. Research and monitoring conducted during the First Increment (2007-2019) suggest width of channel unobstructed by dense vegetation and the distance to nearest forest are the best indicators of roosting habitat suitability (PRRIP, 2017; Baasch et al., 2019). System-scale geomorphology and vegetation monitoring documents trends in channel morphology, vegetation, and WC habitat suitability metrics in relation to natural hydrology, flow releases, and in-channel mechanical management actions. This information is used by the Program to assess our ability to create and maintain suitable whooping crane habitat under a broad range of environmental conditions.

From 2009 – 2016 the Program implemented a field-based monitoring protocol that included topographic transect surveys, vegetation plot surveys, and sediment size/transport sampling (Tetra Tech, 2017). That approach was abandoned after 2016 due to low spatial coverage, increasing cost and the recognition that much of the vegetation and sediment data was not useful for addressing priority uncertainties. In 2017 the Program pivoted to a remote-sensing approach based around collection and analysis of high-resolution aerial imagery and bathymetric LiDAR. To our knowledge, this is the first-time collection of aerial bathymetric LiDAR has been conducted at this scale, frequency, and resolution. Consequently, the Executive Director's Office (EDO) spent much of 2017-2020 collaborating with the Program's remote sensing contractor, Quantum Spatial Inc. (QSI), and working internally to develop and refine analysis methods that could be applied annually at a system scale.

The newly updated remote-sensing data collection and analysis protocol is attached as Appendix A. Protocol implementation includes the following analyses: 1) quantification of management metrics and hydrologic metrics, 2) two-dimensional hydrodynamic modeling to characterize channel hydraulics across a range of discharges, 3) object-based classification of in-channel land cover to characterize changes in in-channel vegetation, 4) topographic differencing to calculate bed volume change, and 5) estimation of suitable whooping crane roosting area. The results of each of these analyses are interpreted relative to Extension Science Plan[1] learning priorities.

1.1 Scope of Analysis and Reporting Scales

The Platte River is a major tributary to the Missouri River with a contributing drainage area of approximately 71,000 square miles (Figure 1). The headwaters of the North and South Platte Rivers are located in the Rocky Mountains and flow eastward to their confluence near North Platte, NE. The central Platte River extends downstream from that point to the Loup River confluence near Columbus, NE. The 90-mile stretch of the Big Bend reach of the central Platte River from Lexington, NE to Chapman, NE is the focus area for Program implementation and is referred to as the Associated Habitat Reach (AHR).

[1] The First Increment AMP has been updated and renamed Extension Science Plan.

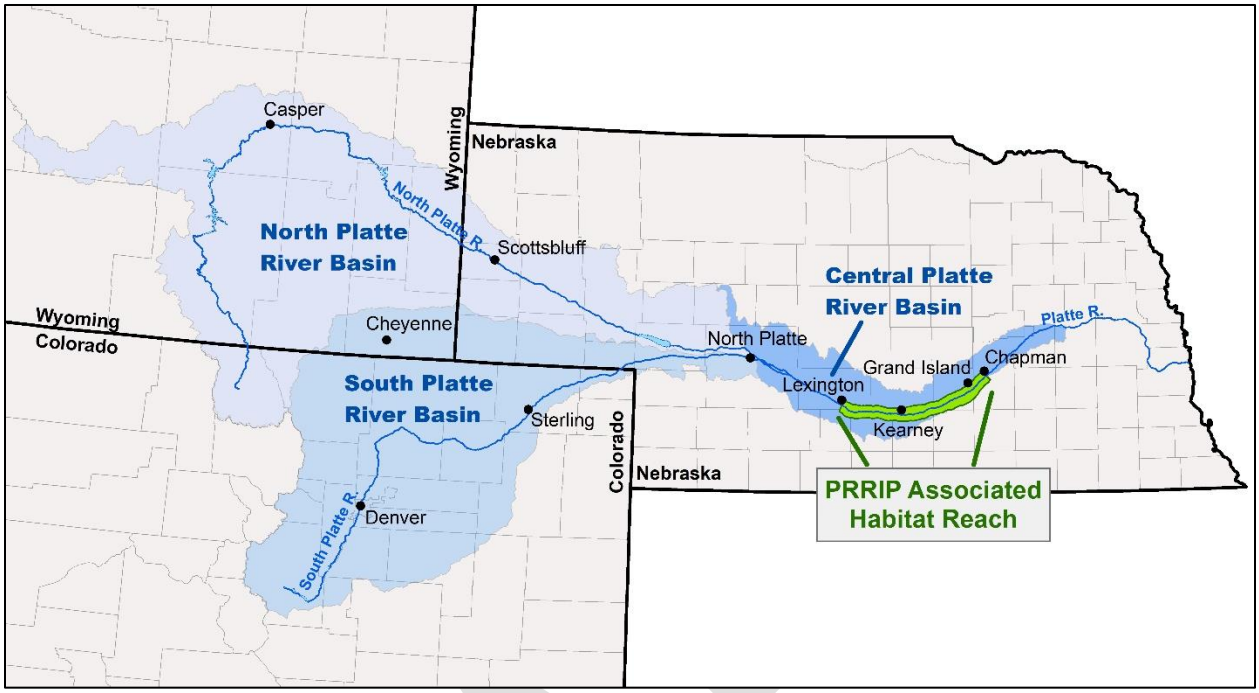

Figure 1. Map of the central and upper Platte River basin including the Program's Associated Habitat Reach (AHR) where management actions are implemented to benefit target species.

Analyses were conducted for the entire AHR and are generally reported at three spatial scales: the entire AHR, by geomorphic reach, and by management type. AHR-scale metrics are reported as means to capture reach-wide annual trends and exclude the two segments (north and south channel) upstream of Overton because they are typically hydrologically disconnected from each other, and the CNPPID J2 Return exerts a controlling influence on reach hydrology.

Geomorphic reaches are based on delineations by Fotherby (2009), grouping segments with similar hydrology and channel morphology into nine (9) reaches (Table 1 and Figure 2). Five of the geomorphic reaches have major flow splits. In those reaches, results are reported for all channels together and the main channel individually[2]. Two additional reaches (Elm Creek to Odessa and Grand Island to Chapman) also have minor flow splits, but no side channels of enough size to be separated in analyses.

Management-scale analyses compare channel characteristics of "managed" and "unmanaged" areas of the main channel. Managed areas include sections of channel managed by PRRIP or other groups that are consistently managed to reduce in-channel vegetation coverage. This includes The Crane Trust, The Audubon Society, The Nature Conservancy, Central Nebraska Public Power and Irrigation District (CNPPID), and the Nebraska Public Power District (NPPD). These areas were delineated using the PRRIP management database, which is described in detail in Section 2.

[2] Suitable whooping crane habitat rarely occurs in side channels due to inadequate width.

Table 1. Geomorphic Reach designations of the AHR, based on Fotherby (2009).

Reach Name	Reach Code	Reach Length (mi)	Geomorphic Description	% Flow in Main Channel
North channel from Lexington Bridge to Overton Bridge	N-lexington_overton	11.3	Wandering: Unconsolidated and heavily vegetated overbank.	25%
South channel J2 Return to Overton Bridge	J2_overton	7.5	Meandering: Incised as much as 25 feet and void of incoming bedload.	75%
Overton Bridge to Elm Creek Bridge	overton_elmcreek	8.7	Unconsolidated: Main channel braided and anastomosed.	75%
Elm Creek Bridge to Odessa Bridge	elmcreek_odessa	7	Consolidated: Braided and anastomosed.	100%
Odessa Bridge to Minden Bridge	odessa_minden	16.7	Unconsolidated: Main channel mostly anastomosed.	55%
Minden Bridge to Gibbon Bridge	minden_gibbon	5.9	Unconsolidated: Main channel braided.	60%
Gibbon Bridge to Wood River Bridge	gibbon_woodriver	15.2	Consolidated: Braided and island braided.	80%
Wood River Bridge to Grand Island (Hwy 34)	woodriver_gi	18.8	Unconsolidated: Main channel mostly braided.	55%
Grand Island (Hwy 34) to Chapman Bridge	gi_chapman	11	Consolidated: Alternating braided and anastomosed.	100%

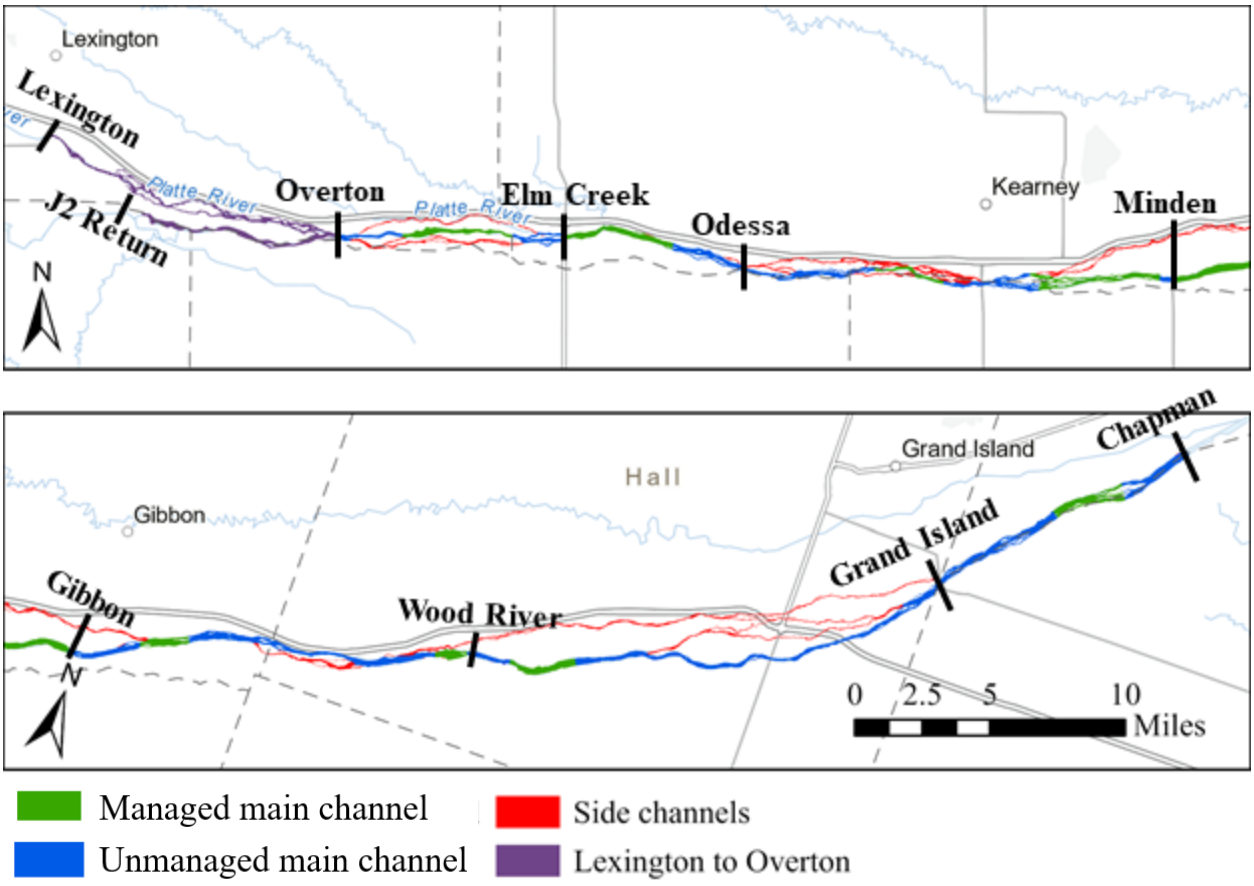

Nebraska Game & Parks Commission, Esri, HERE, Garmin, SafeGraph, FAO, METI/NASA, USGS, EPA, NPS

Figure 2. Map of the Associated Habitat Reach (AHR) including geomorphic reaches, main and side channels, main channel areas that are managed to reduce in-channel vegetation (managed), and other main channel areas (unmanaged).

1.2 Merging Field and Remote Sensing Data and Analyses

The Program has collected and analyzed both field and remote sensing data since 2009. In many cases, the field- and remote-sensing based protocols involve quantification of similar or identical metrics. However, the underlying spatial coverage, data collection methods, and analyses are quite different. It is important that the Program be able to visualize and assess trends since the inception of monitoring. It is also important to identify and avoid situations where changes in methodology could lead to interpretive errors. As such, this report generally presents annual data for the entire system-scale monitoring period of 2009-2020 with the data separated by protocol. In cases where the metrics and results are not comparable, pre-2017 data has been omitted.

1.3 Big Questions and Priority Hypotheses

The Program is currently updating its Adaptive Management Plan (renamed Science Plan) for the First Increment Extension. Draft Science Plan Big Questions and associated hypotheses relevant to geomorphology and vegetation monitoring include:

Big Question 1: How effective is it to use Program water to maintain suitable[3] whooping crane roosting habitat?

- **Management Hypothesis WC1:** During drought periods, 30-day minimum germination suppression releases (2,000 cfs target between June 1-July 15) will slow vegetation expansion into the channel and increase the percent of AHR channel that remains highly suitable for whooping crane roosting.

Big Question 2: How effective is Program management of *Phragmites* for maintaining suitable whooping crane roosting habitat?

- **Management Hypothesis WC2:** During drought periods, 30-day minimum germination suppression releases (2,000 cfs target between June 1-July 15) in combination with continued herbicide spraying and channel disking will slow *Phragmites* rhizome/stolon expansion into the channel and increase the percent of AHR channel that remains highly suitable for whooping crane roosting.

Assumes ongoing phragmites spraying. Program science strongly indicates that natural peak flow events exceeding 13,000 cfs or mechanical vegetation clearing are necessary to remove vegetation and increase maximum unobstructed channel width (MUCW). Channel-inundating flow releases are only hypothesized to maintain unvegetated width.

Big Question 3: Is sediment augmentation necessary to create and/or maintain suitable whooping crane habitat?

- **Management Hypothesis WC6:** Sediment augmentation is necessary to halt the narrowing and incision in the south channel downstream of the J2 Return.

System-scale geomorphology and vegetation monitoring will focus on tracking trends in metrics that are relevant to these Big Questions and associated hypotheses including trends in physical habitat metrics like MUCW as well as potential hydrologic and management drivers. Analyses of management action performance (answering Big Questions) will occur periodically using (in part) physical habitat metric data generated as part of system-scale monitoring.

[3] Channels with ≥ 650 ft maximum width unobstructed by dense vegetation (MUCW) are highly suitable for whooping crane roosting (PRRIP, 2017, Baasch et al., 2019)

2. Mechanical Management

The Program and other organizations mechanically manage in-channel vegetation on both a site and system scale to maintain channel width and provide suitable WC roosting habitat.

- System-scale management actions include helicopter application of herbicide to control invasive vegetation (principally *Phragmites*) and sediment augmentation downstream of the J2 Return to halt channel incision and narrowing in the upper portion of the AHR.
- Site-scale management actions include clearing of trees from in-channel islands and disking of herbaceous vegetation on sandbars and along bank edges. These actions are taken to increase unvegetated channel width and promote channel widening through lateral erosion.[4]

It is important to track these actions to 1) assess their effectiveness, and 2) account for them in analyses of the relationship between natural drivers (such as hydrology) and channel response. Specific management metrics include the spatial extent of annual spraying, woody vegetation clearing and disking as well as the volume of sediment (cubic yards and tons) augmented each year.

2.1 Mechanical Management Analysis Methods

The Program maintains a Geographic Information System (GIS) geodatabase of the spatial extent of vegetation management actions. Table 2 provides the source of GIS data used to document annual management actions in that database. Aerial herbicide application is accomplished by helicopter with boom-mounted global positioning system (GPS) that records the spatial extent of application. Tree clearing and disking areas are recorded via GPS field surveys and track-logs and are then validated with orthorectified imagery collected twice annually. Sediment augmentation area and volumes for each year are calculated using pre- and post-augmentation Light Detection and Ranging (LiDAR) data collected by the Program. Augmentation quantities are validated using RTK-GPS, and area (acres) and volumes (cubic yards/tons) are calculated using a cut-fill routine in GIS for reporting.

Table 2. Data source for documentation of annual system- and site-scale management actions.

Management Action	Data Source
Aerial Herbicide Application	Helicopter applicators equipped with boom-mounted GPS
Tree Clearing	GPS field surveys validated with Program imagery
Disking	GPS track-logs validated with Program imagery
Sediment Augmentation	Pre- and post-augmentation topo-bathy LiDAR surveys

[4] Removing vegetation from bars and bank edges reduces tensile strength of the soil, increasing erodibility (Bankhead, 2012)

Some mechanical management activities occur outside of the active channel. Accordingly, vegetation clearing polygons were clipped to the channel extent using an analysis mask developed for the object-based land cover classification, as described in Section 5.

2.2 Mechanical Management Results

Most mechanical management during the period of 2006 - 2020 was comprised of aerial herbicide application and disking with tree clearing occurring on a much smaller scale (Figure 3). The period of 2006 – 2009 coincided with the end of a historic drought in the basin and the associated proliferation of *Phragmites* into the river channel. Aerial herbicide application to control *Phragmites* began in 2007, peaked in 2009, and has been relatively constant since 2016 at approximately 500 acres per year. We hypothesize that this is the baseline level of treatment that is necessary to prevent *Phragmites* from reinfesting the channel. It is not certain whether baseline effort will need to increase during dry periods or if the continual annual control effort has normalized the amount of treatment for all year types.

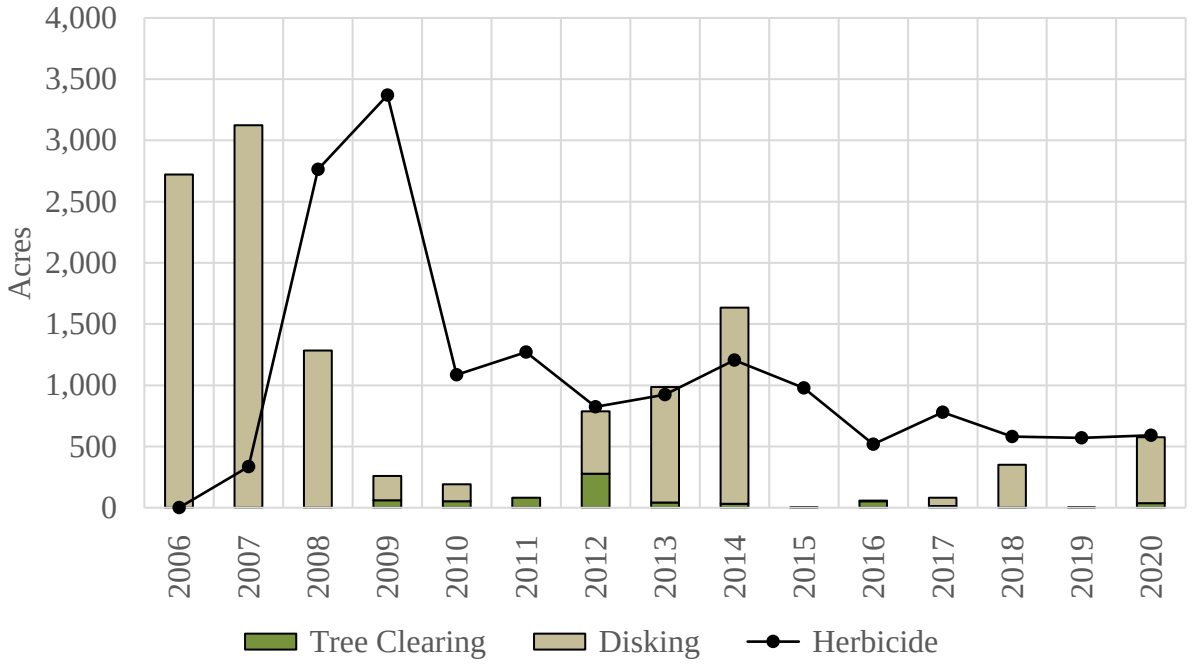

Figure 3. Total area of in-channel tree clearing, river channel disking and aerial herbicide application by year for the AHR.

See Appendix Section B for complete mechanical management results.

3. Hydrologic Analysis

Flow is a primary driver of annual changes in channel characteristics on the Platte (Murphy et al., 2004, Farnsworth et al., 2018). The magnitude, timing, and duration of flows drive complex relationships with in-channel vegetation and sediment transport. For example, high peak flows in any season can scour vegetated sandbars and collapse banks. Lower flows sustained over a long period in the growing season can suppress seed germination. Both types of flow suppress vegetation and support unvegetated channel width, though through different physical processes. The hydrologic metrics included in this report have all been hypothesized to have distinct spatiotemporal effects on in-channel habitat.

3.1 Hydrologic Metrics

Priority hydrologic metrics are presented in Table 3 and a larger suite of hydrologic metrics, including flow duration curves and exceedance percentiles for germination and WC migration seasons are reported in Appendix C. Priority metrics including mean annual discharge (Q_{AVG}), annual flow volume (V_{af}) and peak flow discharge/return interval (Q_P/Q_{Py}) are indicators of general hydrologic conditions in the reach. The Annual 40-day maximum flow ($Q_{Max\ 40}$) has been found to be a good predictor of increases in unvegetated channel width (PRRIP, 2017) and mean June flow (Q_{June}) is hypothesized to be a good predictor of channel width maintenance in years absent large peak flow events. Flow distribution curves are also provided as a general indicator of the distribution of mean daily discharge within each year (Appendix C).

Table 3. Priority hydrologic metrics, symbols and importance.

Metric	Metric Symbol	Utility
Mean Annual Discharge (cfs)	Q_{AVG}	Indicator of general hydrologic conditions
Annual Flow Volume (AFY)	V_{af}	Indicator of general hydrologic conditions
Annual Mean Daily Peak Discharge (cfs)	Q_P	This is the annual peak flow discharge. Mean daily flow is used because it occurs for a sufficient duration to do work within the channel.
Annual Peak Flow Return Interval (years)	Q_{Py}	Indicator of how frequently peak flow magnitudes occur
Annual 40-Day Maximum Flow (cfs)	$Q_{Max\ 40}$	Indicator of peak flow magnitude-duration relationship; good predictor of unvegetated channel width increases
Mean June Flow (cfs)	Q_{June}	Hypothesized to be good predictor of unvegetated channel width maintenance in absence of peak flow events
Flow Distribution Curves	NA	Distribution of mean daily discharge within the year

3.2 Hydrologic Analysis Methods

Mean daily discharge records were obtained for two United States Geological Survey (USGS) stream gages located at Overton (06768000) and Grand Island (06770500) for the period of 2009-2020. Metric values were calculated for each gage location. Annual peak flow return interval was calculated using the methodology from USGS Bulletin #17B (Interagency Advisory Committee on Water Data, 1982). We used a period of record of 1958-2020 for return interval calculations as the last major reservoir on the North Platte River was completed in 1957.

3.3 Hydrologic Analysis Results

Mean daily discharge at the Grand Island gage (06770500) for the period of geomorphology and vegetation monitoring (2009-2020) is plotted in Figure 4. During this period, mean annual discharge ranged from a low of 942 cfs at Overton in 2009 to a high of 4,214 cfs at Grand Island in 2011 (Table 4 and Table 5).

Mean daily peak discharge since initiation of system-scale monitoring ranged from a low of 2,960 cfs at Overton in 2018 to a high of 18,200 cfs at Grand Island in 2019 (Table 4 and 5). The 2019 Grand Island peak had a 24-year return interval. Other notable peaks included a long-duration peak in 2011 with an approximately 5-year return interval and 2013 and 2015 peaks with 15-year return intervals. Notably, all large peaks occurred in late spring except for the 2013 event which occurred in the fall due to a historic precipitation event in the upper South Platte basin. The median of the mean daily peak discharge for the reporting period is approximately 8,700 cfs.

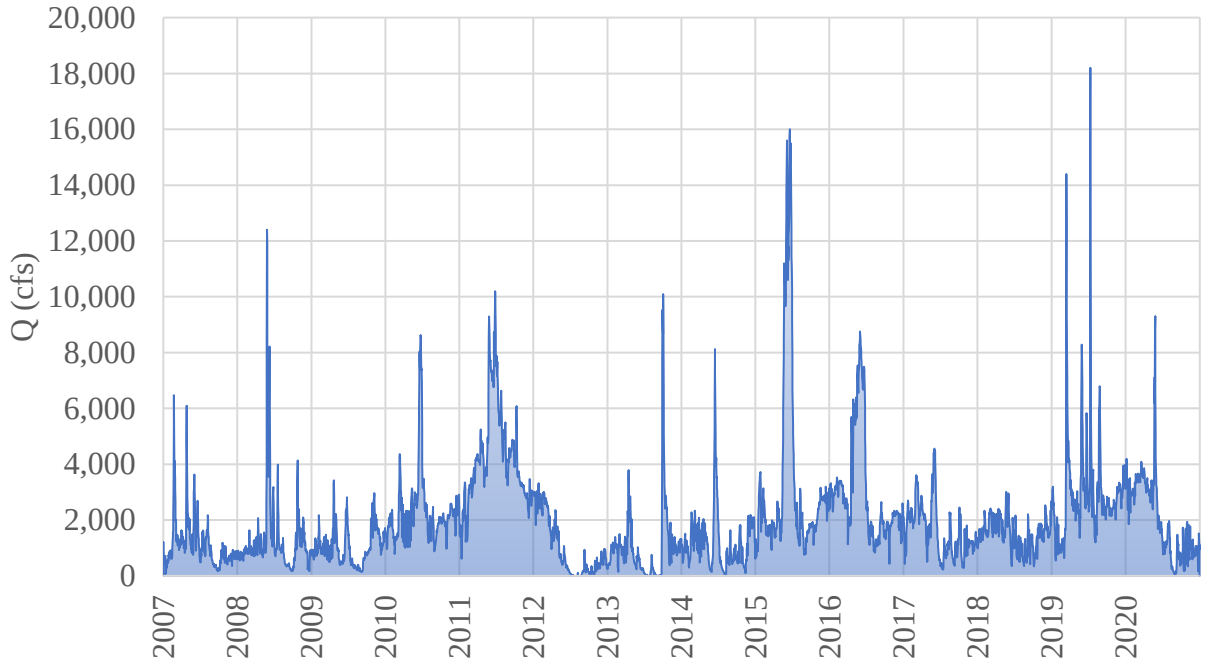

Figure 4. Mean daily discharge at the USGS Grand Island (06770500) gage.

Table 4. Summary of flow metrics at the USGS Overton (06768000) gage from 2009 to 2020. Years of remote monitoring are shown in green.

Water Year	Mean Annual Discharge	Annual Volume (ac-ft)	Mean Daily Peak Discharge	Return Interval (Years)	40-Day Max Discharge	Mean June flow (germination)
Mean 1958-2020	1,706	1,235,039	6,401	4.2	3,775	2,711
2009	942	681,929	3,600	1.5	1,811	1,282
2010	2,157	1,561,636	7,370	3.4	4,108	4,536
2011	3,877	2,807,021	8,720	4.6	7,503	7,675
2012	1,114	806,776	3,430	1.4	2,796	319
2013	1,140	824,993	12,400	9.9	4,129	303
2014	1,249	904,099	7,360	3.4	3,150	3,822
2015	3,506	2,538,110	15,300	16.6	12,708	12,920
2016	2,950	2,137,701	8,600	4.5	7,364	6,433
2017	1,550	1,122,462	4,440	1.8	2,768	2,069
2018	1,415	1,024,113	2,960	1.3	1,834	1,343
2019	2,274	1,646,137	9,750	5.6	3,089	2,822
2020	1,802	1,305,700	3,820	1.5	2,977	1,966

Table 5. Summary of flow metrics at the USGS Grand Island (06770500) gage from 2009 to 2020. Years of remote monitoring are shown in green.

Water Year	Mean Annual Discharge	Annual Volume (ac-ft)	Mean Daily Peak Discharge	Return Interval (Years)	40-Day Max Discharge	Germination (June)
Mean 1958-2020	1,749	1,266,672	7,370	4.5	3,977	2,841
2009	1,039	752,027	3,430	1.2	2,011	845
2010	2,289	1,657,360	8,630	3.3	4,960	3,126
2011	4,214	3,050,549	10,200	4.6	7,982	6,216
2012	978	709,145	3,320	1.2	2,857	630
2013	1,024	741,203	10,100	4.5	3,524	575
2014	1,199	867,918	8,120	3	2,778	1,474
2015	3,341	2,418,834	16,000	14.9	12,636	9,116
2016	2,993	2,168,546	8,750	3.4	7,390	7,057
2017	1,585	1,147,310	4,560	1.5	2,943	2,752
2018	1,502	1,084,571	3,010	1.2	2,036	1,888
2019	3,008	2,176,267	18,200	24	4,615	3,609
2020	2,005	1,453,271	9,310	3.8	3,755	3,471

See Appendix Section C for complete hydrologic results.

4. Hydrodynamic Modeling

Two-dimensional hydrodynamic modeling is used to estimate water surface elevation, velocity and other hydraulic metrics at a variety of flows based on bathymetric LiDAR-derived channel topography. Modeled hydraulic metrics are used to estimate changes in width, depth, and area of shallow water, all of which are important elements of in-channel WC habitat.

4.1 Hydrodynamic Modeling Methods

Two dimensional (2-D) hydrodynamic models compute water-surface elevation and other hydraulic metrics from an elevation surface derived from annual topobathymetric LiDAR surfaces. Modeling was performed using the Bureau of Reclamation (BOR) SRH-2D Version 2.2 (BOR, 2008) solver with Version 13.1 of the Aquaveo Surface Water Modeling System (SMS) graphical user interface (Aquaveo, 2010). SRH-2D provides a significant advantage over most 2-D models because the density of the computational points can be increased in complex active channels areas and decreased in others to maintain reasonable model size and computational efficiency. The AHR was subdivided into six sub-models (Figure 5), rather than the nine geomorphic reaches, to reduce processing and computation time. Topobathymetric LiDAR surfaces were processed into a computational mesh with model node spacing of approximately 20 feet, in accordance with the BOR SRH-2D guidelines (BOR, 2008).

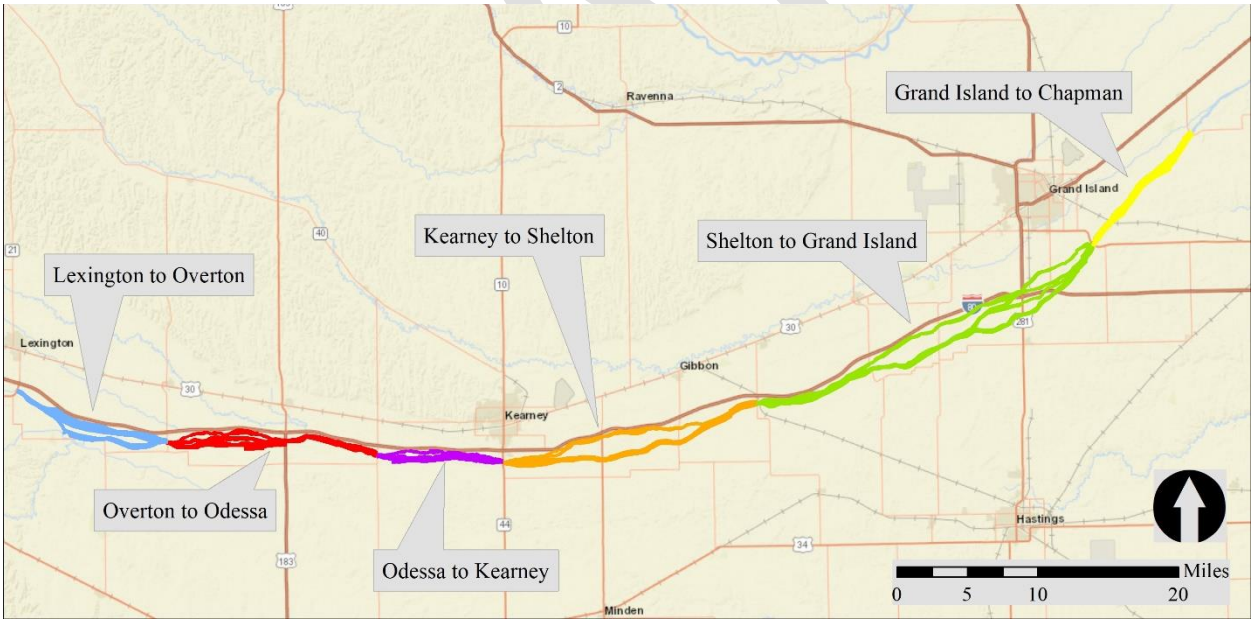

Figure 5. Hydrodynamic sub-models within the AHR.

The SRH-2D model utilizes Manning's roughness coefficients to represent channel roughness. Since all flow is confined to the active channel at discharges of interest (for this analysis), a single roughness coefficient was used for each reach model. The coefficient was calibrated by iteratively adjusting the value until modeled stage converged to field measurements. The calibrated model was then validated to a second discharge and measured water surface elevation. A comparison of modeled and LiDAR-measured water surface elevations (Table 6) indicates all but one modeled

water surface elevation fall within +/- 0.2 ft of measured values. Values of NA in the table represent areas without validation points. Since the modeling effort began, we have worked to develop access to a series of stable channel locations to measure validation points that cover all sub-model reaches.

Table 6. Predicted water-surface elevations minus LiDAR-measured water-surface elevations (ft) for all models 2017-2020.

Sub-Reach	2017	2018	2019	2020
Lexington to Overton	NA	0.14	-0.06	-0.02
Overton to Odessa	NA	-0.15	-0.11	0.1
Odessa to Kearney	0.23	-0.07	0.13	-0.06
Kearney to Shelton	0.17	-0.04	-0.1	-0.06
Shelton to Grand Island	-0.07	-0.09	0.09	-0.01
Grand Island to Kearney	NA	NA	0.18	-0.07

SRH-2D model output was processed with both R (R Core Team, 2017) and GIS to calculate hydraulic metrics of interest (Table 7). Wetted width was calculated by sampling the model area extent with transect lines spaced at 500 ft. intervals. Other metrics were calculated through tabular manipulation in R. More detail on these methods can be found in Appendix A1.

Table 7. Subset of useful hydrodynamic metrics parameterized from the reach-wide hydrodynamic modeling results.

Metric	Utility
Percent flow consolidated in main channel at 2,000 cfs	Important for assessing relationship between flow and channel width metrics in split flow reaches.
Mean depth at 2,000 cfs	Important reference for incision
Mean wetted width at 2,000 cfs	Important for assessing relationship between wetted width and vegetation germination
Width:depth ratio at 2,000 cfs	Higher values reflect higher degree of braiding
Wetted area at 5,000 cfs	Used to mask in-channel area for clipping total unobstructed channel width (TUCW)
Area with Depth < 1ft	Important whooping crane habitat metric

4.2 Hydrodynamic Modeling Results

A plot of the 2020 modeled wetted width of all channels at 2,000 cfs (Figure 6) indicates that width is highly variable throughout the AHR but generally increases in a downstream direction. A plot of the 2020 modeled wetted width of the main channel (Figure 7) does not show the same increasing downstream trend, in part because wetted with of the main channel is strongly influenced by the proportion of flow that is consolidated into the main channel at any given location.

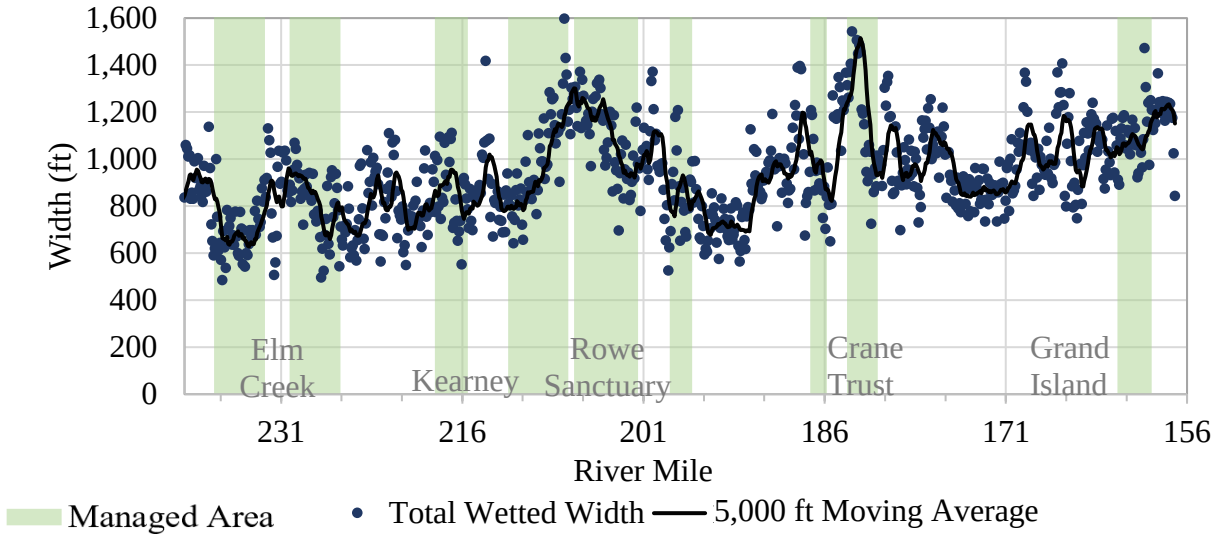

Figure 6. All channels wetted width, as sampled at 500 ft transect intervals from the 2000 cfs 2020 hydrodynamic model.

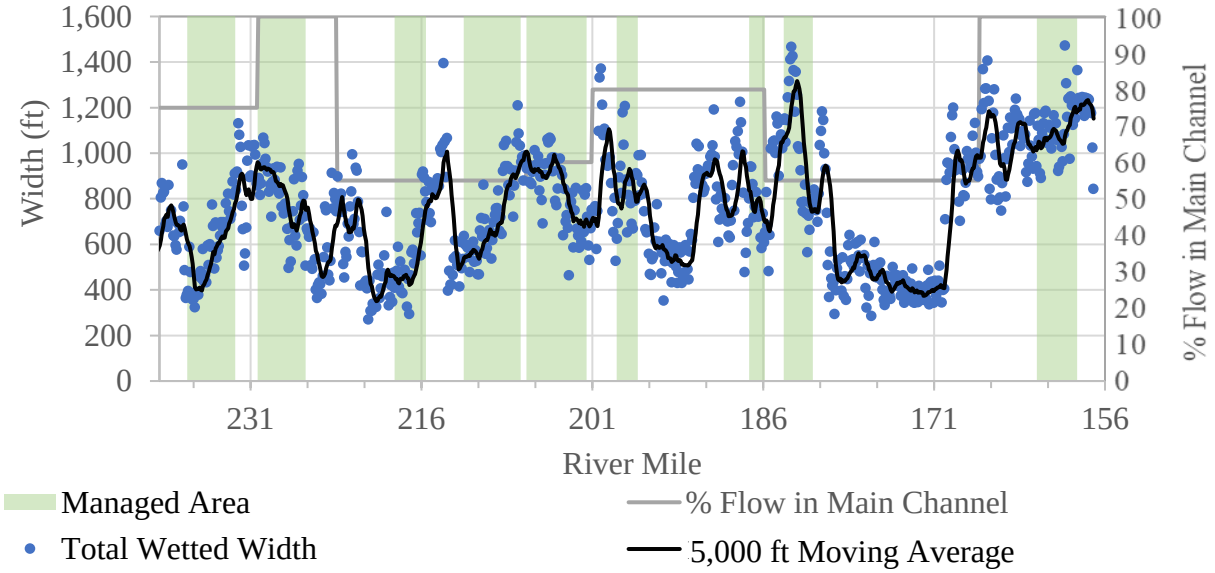

Figure 7. Main channel wetted width, as sampled at 500 ft transect intervals from the 2000 cfs 2020 hydrodynamic model.

Comparing managed areas to other areas of the main channel provides a cursory indication of the effect of management on morphology. Managed areas have, on average, slightly higher width, lower depth, and a higher width:depth ratio than other areas. However, the differences are small. The differences in wetted width are well within the bounds of the standard error of the distribution (Figure 7). The 2019 floods did not appear to substantially change channel hydraulics. However, in 2019, managed areas did experience a small increase in average depth and corresponding decrease in the width:depth ratio. Overall, year-to-year differences are small and indicate that the morphology of the AHR did not change substantially from 2017-2020.

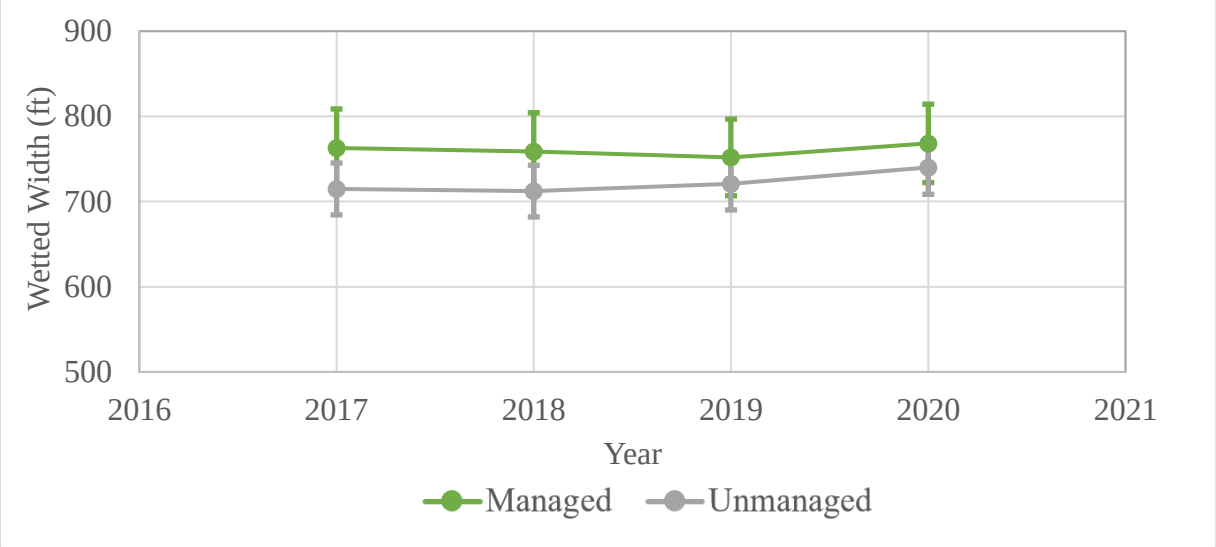

Figure 8. Mean (points) and standard error (bars) of wetted width over time from Overton to Chapman in areas of the main channel managed to reduce in-channel vegetation (managed) and other main channel areas (unmanaged). Data are sampled at 500 ft transect intervals from the 2000 cfs 2020 hydrodynamic model.

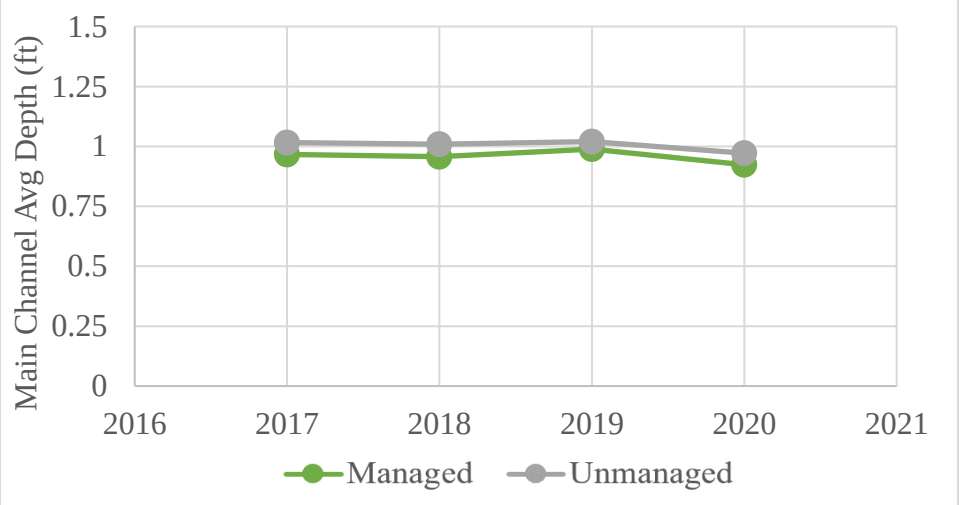

Figure 9. Mean depth over time from Overton to Chapman, from the 2000 cfs 2020 hydrodynamic model in areas of the main channel managed to reduce in-channel vegetation (managed) and other main channel areas (unmanaged).

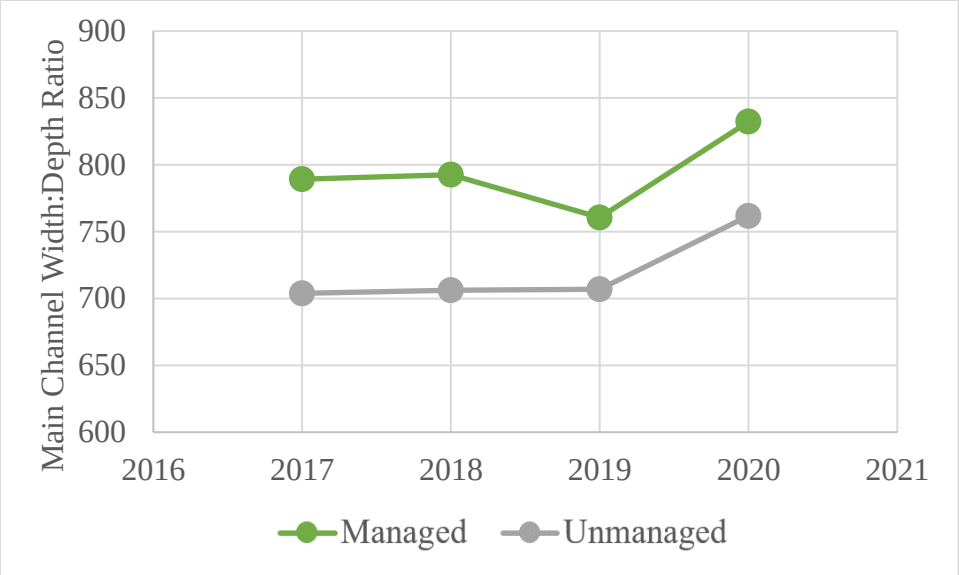

Figure 10. Width:depth ratio over time from Overton to Chapman, from the 2000 cfs 2020 hydrodynamic model in areas of the main channel managed to reduce in-channel vegetation (managed) and other main channel areas (unmanaged).

The modeling results also allow for the examination of the area of channel with depth less than 1 ft, which is an important component of WC roosting habitat. Results indicate that the area of shallow channel is maximized at a flow of 750 cfs (Figure 11). At 2,000 cfs, the percentage of the total channel area < 1 ft deep was slightly higher in managed areas (Figure 12). Shallow channel area increased every year in managed areas and did not appear to be strongly influenced by the 2019 floods. Shallow channel area did not increase as much in unmanaged areas.

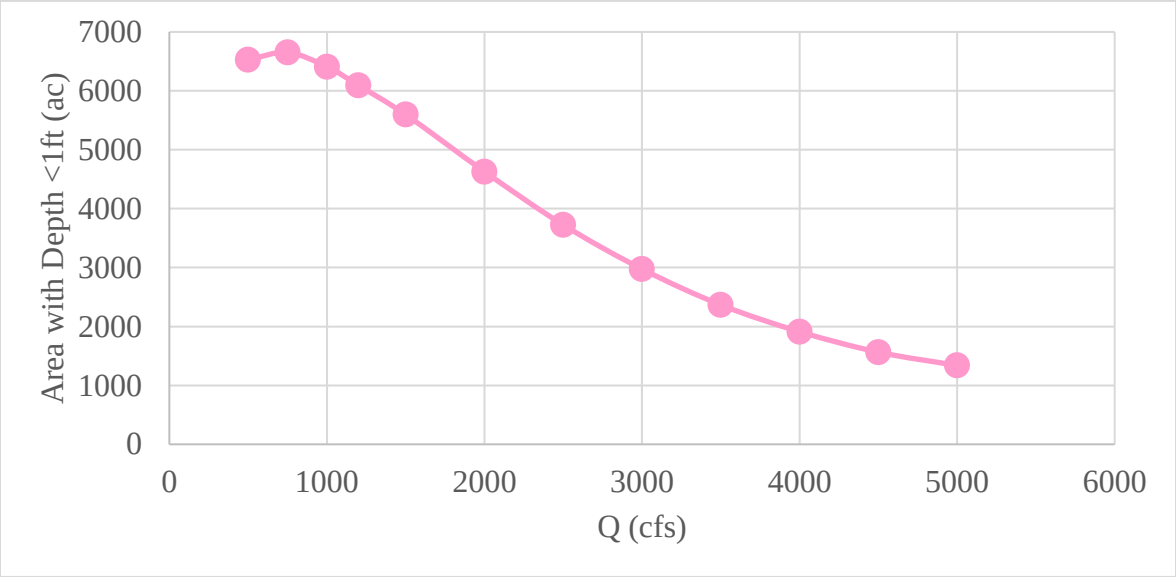

Figure 11. Total channel area from Overton to Chapman with depth less than 1 ft, as estimated with the 2020 hydrodynamic model.

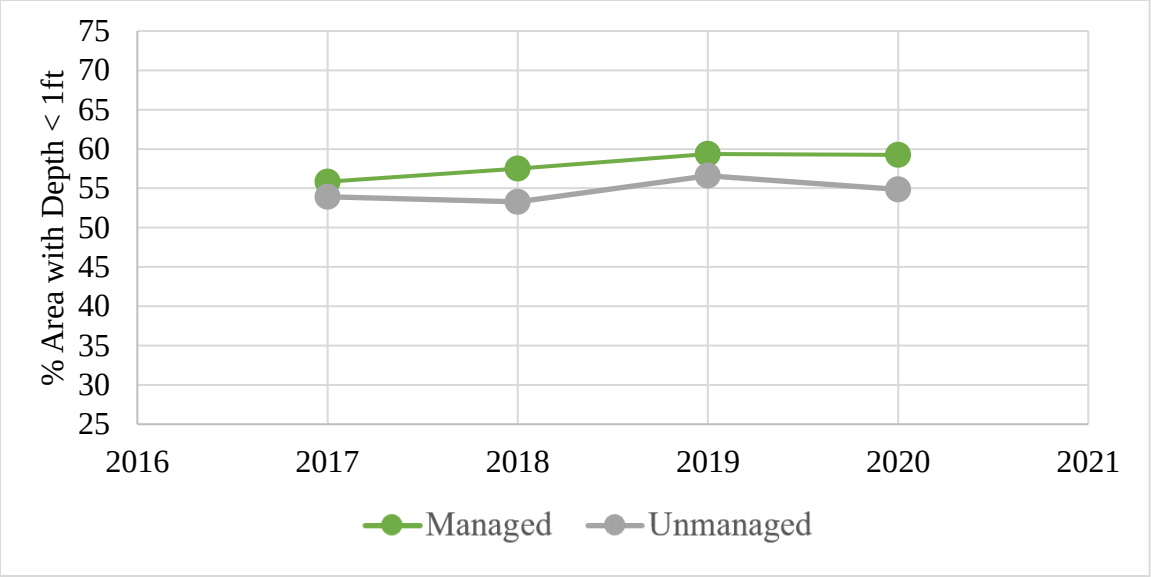

Figure 12. Percentage of channel area with depth less than 1 ft at 2000 cfs in areas of the main channel managed to reduce in-channel vegetation (managed) and other main channel areas (unmanaged) as estimated from 2017-2020.

See Appendix Section D for complete hydrodynamic modeling results.

5. Land Cover Classification

Quantifying land cover change over time is critical for understanding changes in PRRIP target species habitat and measuring the success of management. The land cover classes included in this protocol are water, sand, and vegetation of various height classes. Analyzing trends in coverage of each class can provide important information about vegetation dynamics in the AHR. From a WC habitat perspective, the most important aspect of classification is defining areas of the channel that are unobstructed (water, sand, or vegetation less than 2 ft in height) or are obstructed by vegetation greater than or equal to 2 ft in height.

Channel width that is unobstructed by tall vegetation is evaluated in two different ways. Maximum unobstructed channel width (MUCW) represents the maximum continuous channel width that is unobstructed by vegetation ≥ 2 ft in height. It is a good predictor of whooping crane roost location (Baasch et al., 2019). Total unobstructed channel width (TUCW) represents the total of all segments of channel width unobstructed by vegetation ≥ 2 ft in height. TUCW is an important physical process metric (Farnsworth et al., 2018) as it is less impacted by the orientation of vegetated obstructions within the active channel.

5.1 Land Cover Classification Methods

From 2009-2016, field crews estimated MUCW and TUCW in the field at anchor point locations via field surveys. PRRIP researchers have also estimated MUCW and TUCW from annual aerial imagery by visually identifying unvegetated channel segments at predetermined transect locations (Farnsworth et al., 2018).

From 2017 forward, object-based classification of land cover class from annual aerial imagery will be used as a replacement for visual classification. Object-based classification is an automated algorithmic method that can interpret remote sensing data, categorizing it into predefined land cover classes. It offers several advantages over visual classification by removing the potential for observer bias, simultaneously incorporating both elevation and imagery data, and improving repeatability among years.

The remote sensing data used for classifications was collected via airplane by Quantum Spatial, Inc. (QSI) in either October or November from 2017-2020. Processed coverages include 4-band (red, green, blue, and near-infrared) imagery (Figure 13a) and LiDAR elevation surfaces representing both the bare earth and the top of vegetation used to derive vegetation height (Figure 13b). QSI assessed accuracy for each year of data collection using ground control check points (QSI, 2016; QSI, 2017; QSI, 2018; QSI, 2019; QSI, 2020). The elevation vertical accuracy, presented here as a 95% confidence interval for elevation estimates, varied from 0.1 to 0.2 ft between years on dry, unvegetated surfaces (Table 16).

Land cover classification was accomplished using Trimble eCognition object-based classification software (Trimble, 2021). In object-based classification, pixels are grouped into spectrally homogenous objects, and then the objects are classified utilizing user-defined criteria. This method differs from the more traditional pixel-based classification, in which all pixels are classified by their individual spectra (Burnett & Blaschke, 2003). Object-based classification has been

demonstrated to be more effective than pixel-based classification in a wide variety of environments (Blaschke, 2010), and a powerful tool for specifically classifying patches of in-channel vegetation on sandbars (Demarchi et al., 2016).

The land cover classification schema incorporated 6 classes as defined in Table 8. Both the imagery and elevation data were classified at 3 ft spatial resolution. Water and sand were differentiated from vegetation using the Normalized Difference Water Index (NDWI) and Normalized Difference Vegetation Index (NDVI). NDWI and NDVI are indices combining reflectance in the green and near-infrared bands (McFeeters, 1996), and the red and near-infrared bands (Rouse et al., 1973), respectively. NDVI values range from -1 to 1 and are positively correlated with leaf density and health (Rouse et al., 1973). NDWI values also range from -1 to 1, with positive values representing water (McFeeters, 1996).

Water was differentiated from land using the NDWI and sand was differentiated from short vegetation using NDVI. The cutoff values for both indexes were visually calibrated for each year—values are presented in Table E1 in Appendix E. Annual NDVI calibration is necessary due to the impact of climactic variations on vegetation health. Vegetation was then differentiated into height classes using the LiDAR vegetation height surface (Figure 13b). This process generated a reach-wide map of land cover classes as shown in Figure 13c. In-channel land cover classes less than 2ft in height were considered unobstructed, that is, they were not considered as presenting a visual obstruction to whooping cranes utilizing the channel. Typical vegetation included in each vegetation height class can be found in Table 8.

Table 8. Land cover classes derived from object-based classification, obstructed or unobstructed classification, and typical vegetation type.

Land Cover Class	Obstructed/ Unobstructed	Typical Vegetation Class
Area of Sand and Water	Unobstructed	Unvegetated
Area of Vegetation < 2 ft	Unobstructed	Sparse or dense short herbaceous
Area of Vegetation 2 – 6 ft	Obstructed	Tall herbaceous or *Phragmites*
Area of Vegetation 6 – 15 ft	Obstructed	*Phragmites* or woody vegetation
Area of Vegetation > 15 ft	Obstructed	Woody vegetation

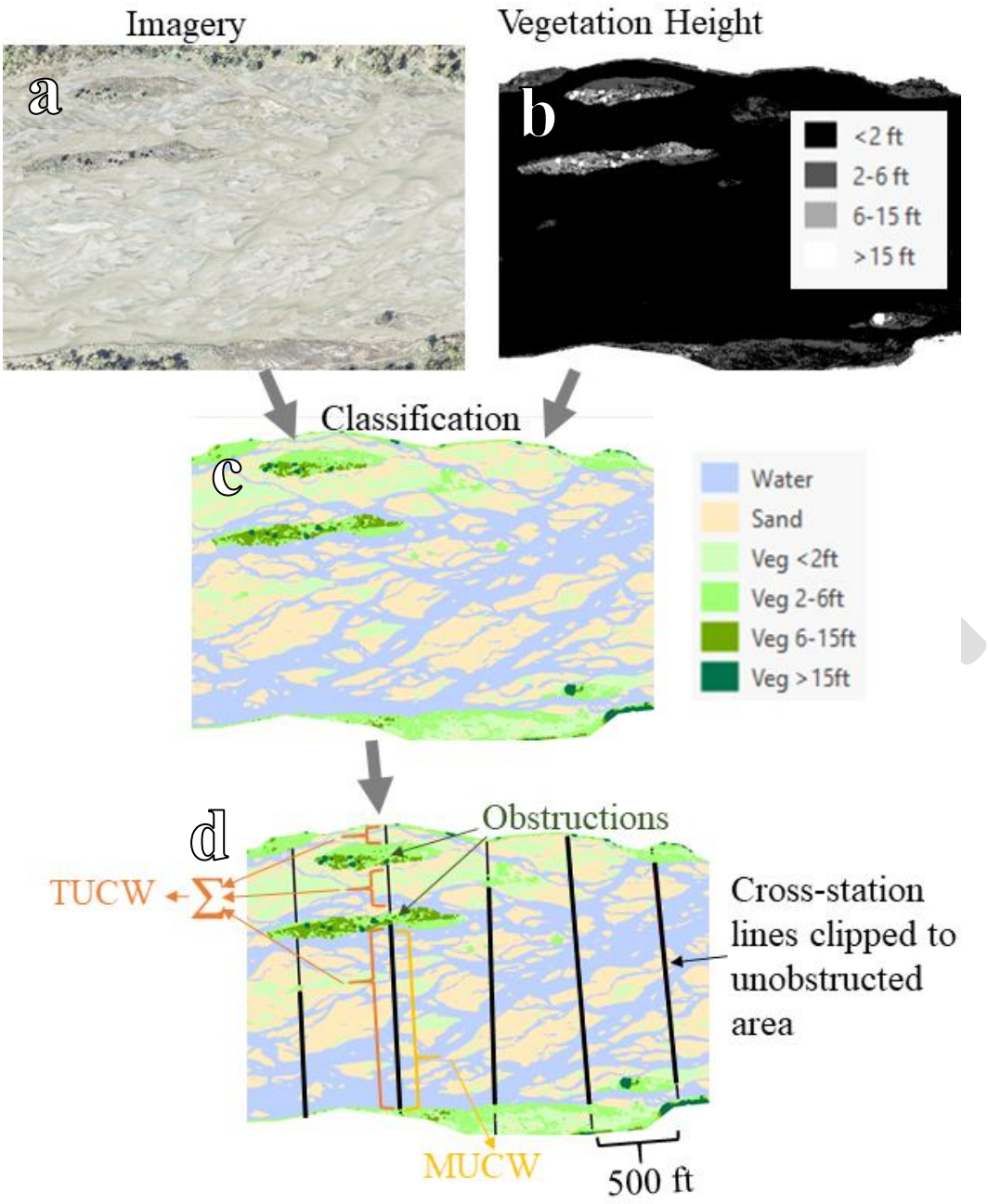

Figure 13. Conceptual diagram illustrating the combination of (a) imagery and (b) LiDAR-derived vegetation height data to (c) classify land cover surface. The land cover surface is then used to (d) clip cross-station lines to unobstructed area, calculate MUCW as maximum continuous channel width that is unobstructed by vegetation ≥ 2 ft in height, and calculate TUCW as the total of all segments of channel width unobstructed by vegetation ≥ 2 ft in height.

Classification analyses were validated by comparing object-based classification results to field data. For best comparison, field validation points were collected within a week of the data collection flight. A total of 440, 157, and 124 validation points were collected by the EDO in 2018,

2019, and 2020, respectively. Field data were also collected in 2017, but according to a preliminary classification schema that was not ultimately used, the data from that year were unsuitable for a validation analysis. Complete confusion matrices presenting comparisons between object-based classifications and field classifications are presented in Tables E2, E3, and E4 in Appendix Section E.

The comparison analysis indicated obstructed /unobstructed area agreement exceeded 80% in all years and 90% in two out of three years (Table 9). The most common error was classification of points identified in the field as tall vegetation (> 2 ft) as some shorter class of vegetation. This error is likely a result of the spatial scale of the remote sensing data. The vegetation height rasters used in analysis represent the average elevation of the LiDAR point cloud within each 3 ft x 3 ft cell. If a vegetation patch is small or sparse, the highest points may be averaged out to a lower value at the point of conversion from LiDAR point cloud to raster. A cell that contains a sparse or partial patch of vegetation 6-15 ft in height, for example, may have an average elevation value lower than 6 ft.

Table 9. Result of comparisons between object-based land cover classification and field classification by year.

Year	Total Classification Agreement (among all classes)	Percent of Disagreement Attributable to Vegetation Height Underestimate	Obstructed/ Unobstructed Agreement
2017	N/A	N/A	N/A
2018	86%	89%	91%
2019	82%	90%	82%
2020	94%	57%	98%

Land cover classification maps were used to identify the total area of each class and to calculate MUCW and TUCW (Figure 13d and Table 10). MUCW and TUCW were extracted by spatially clipping cross-station lines spaced at 500 ft intervals throughout the AHR to the area of unobstructed classes—water, sand, and vegetation less than 2 ft in height (Figure 13d). TUCW was additionally clipped to the 5,000 cfs flow extent to prevent unvegetated line segments from extending overbank. MUCW was then measured at each of the clipped cross-station lines as the maximum continuous channel width that is unobstructed by vegetation ≥ 2 ft in height. TUCW was measured at each of the clipped cross-station lines as the total of all segments of channel width unobstructed by vegetation ≥ 2 ft in height. Mean values of each metric were then calculated at various spatial scales to examine larger-scale trends.

Table 10. Habitat metrics derived from land cover classifications that are important for whooping cranes.

Metric	Metric Symbol	Definitions
Maximum Unobstructed Channel Width	MUCW	The longest continuous channel width unobstructed by vegetation ≥ 2 ft in height
Total Unobstructed Channel Width	TUCW	Sum of all segments of channel width unobstructed by vegetation ≥ 2 ft in height
Percent Unobstructed Area		Percent area of the channel unobstructed by vegetation ≥ 2ft in height

Mean MUCW and TUCW were calculated for all channels together and the main channel individually. Past PRRIP analyses have focused on MUCW of all channels—which is almost exclusively located in the main channel— and TUCW of the main channel as being most relevant to WC.

5.2 Continuity With Older Data

While object-based classification will serve as the principal method for measurement of in-channel vegetation from 2017 onward, either the pre-2017 visual remote sensing classification or field-surveyed data must be used in tandem with the newer data to capture longer-term changes. Large-scale differences in most years are evident when results from field surveys and visual remote sensing classification are compared for both MUCW (Figure 14) and TUCW (Figure 15). In many years, the difference in the mean values is as much as 200-300 ft.

These discrepancies can be ascribed to several differences between methods including the field survey extending MUCW past the edge of channel into the overbank; the remote sensing visual classification of vegetation height without elevation data; differing delineation of the channel bank location; as well as the limited sample size of the field survey transects compared to the remote sensing transects. Because visual classification is most like the object-based classification in terms of both measurement methods, spatial coverage, and sample size, the visual classification will be used going forward to report channel widths prior to 2017.

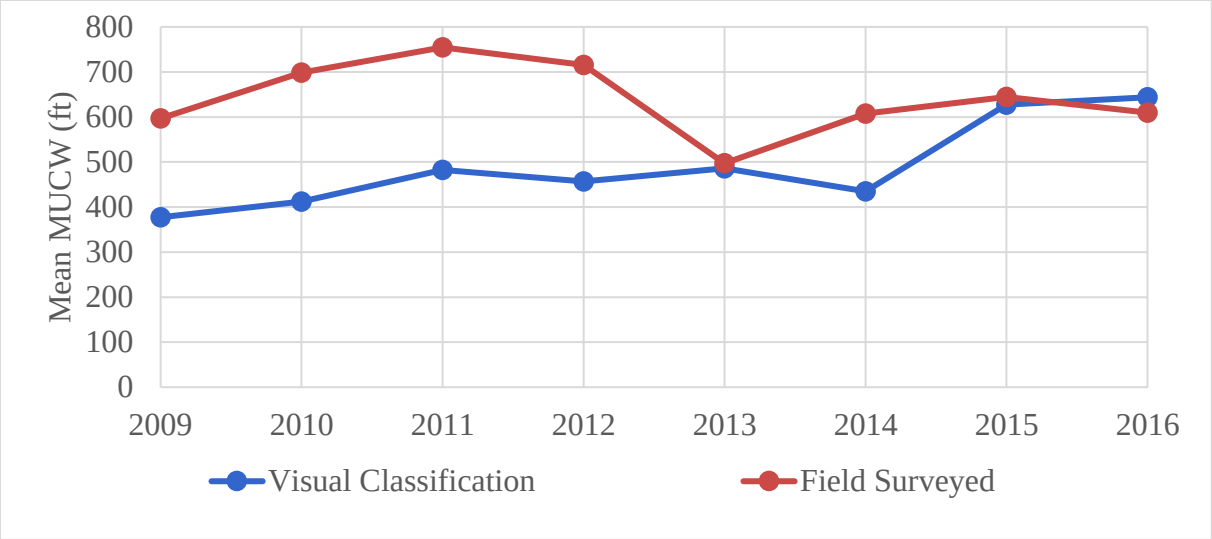

Figure 14. Comparison of the mean MUCW over all channels as measured with visual classification and field surveys from 2009-2016.

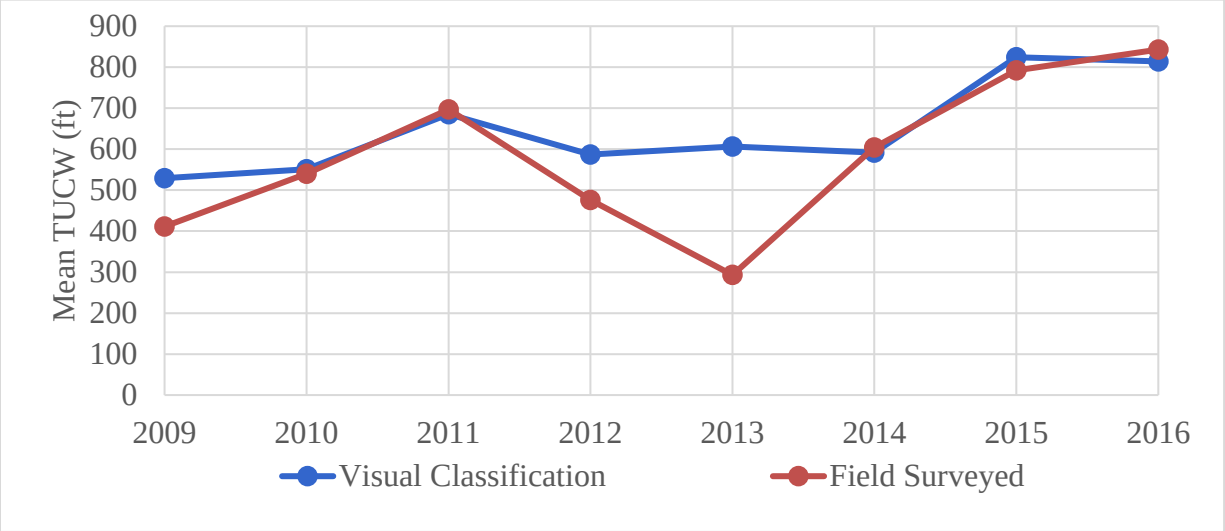

Figure 15. Comparison of the mean TUCW of the main channel as measured with visual classification and field surveys from 2009-2016.

Object-based and visual classification results for MUCW and TUCW were compared for the period of 2017-2020 (Figure 16) to evaluate the similarity of estimates from the two methodologies. Paired t-tests were used to compare results from the two methods using the same subset of originally sampled transects at 5,000 ft spacing to reduce spatial autocorrelation.

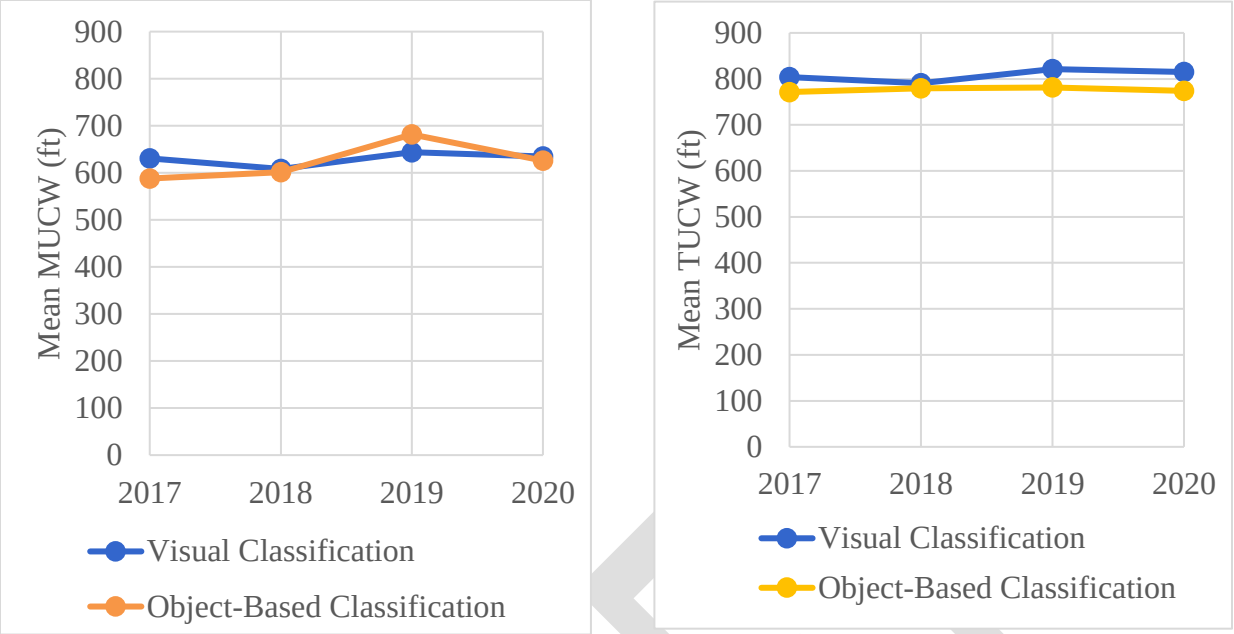

Figure 16. Mean MUCW (all channels) values (left) and TUCW (main channel) values (right), as measured with visual classification and object-based classification for the years 2017-2020.

Object-based classification unobstructed channel widths were typically narrower than visually classified channel widths from 2017-2020, but differences constituted a small percentage of widths. Mean estimates of object-based classification MUCW were significantly narrower in 3 of 4 compared years, with the largest average difference of 52 ft, or 9% of the average, occurring in 2017 (Table 11). Mean estimates of object-based classification TUCW were also significantly narrower in 3 of 4 compared years, with the largest average difference of 33 ft, or 4% of the average, occurring in 2017 (Table 12). Overall, the limited, predictable channel width measurement differences between object-based and visual classifications will allow for effective analysis of large-scale, long-term trends using visual classifications prior to 2017 and object-based classification starting in 2017.

Table 11. Comparing object-based and visual classification estimates of MUCW estimates along the same transects. P values were calculated using paired t-tests within each year.

Year	Est. Mean Diff. Ecog-Visual (ft)	Diff. % of Mean	Difference 95% Confidence Interval (ft)	p value
2017	-52	9	-83 : -22	<0.01
2018	-22	4	-52 : 7	0.13
2019	39	6	5 : 72	0.03
2020	-21	3	-40 : -2	0.03

Table 12. Comparing object-based and visual classification estimates of MUCW and TUCW estimates along the same transects. P values were calculated using paired t-tests within each year.

Year	Est. Mean Diff. Ecog-Visual (ft)	Diff. % of Mean	Diff. Confidence Interval (ft)	p value
2017	-33	4	-49 : -18	<0.01
2018	-2	0	-20 : 16	0.82
2019	-29	4	-43 : -14	<0.01
2020	-28	3	-46 : -9	<0.01

The systematic difference between visual and object-based classification may in part due to the lack of elevation or vegetation height data in the visual classification methods. Visual observers rely primarily on vegetation density to interpret vegetation height. One land cover that exemplifies potential problems with this method is grass. In-channel grasses on the Platte may range from 0-6 ft tall and at any height may be highly variable in color and density (Figure 17). Determining whether each patch is greater or less than 2 ft based on visual interpretation of aerial imagery alone is inherently subjective.

Figure 17. Three patches of in-channel grass observed on the Platte in November of 2021 with variable height, density, and color. Researcher is 6 ft tall.

There are other factors that may explain the systematic difference between the visual and object-based classification results, including the subjective nature of bank delineation by visual observers, and the scale of visual observation. Visual observers typically draw out unobstructed width lines at a scale of 1:2,400. At that scale, visual observers may miss small patches of obstructing vegetation, resulting in overextension of unobstructed width lines. Whatever its cause, the systematic difference between the two methods is small, which indicates that large-magnitude trends in MUCW and TUCW are detectable when incorporating results from the two methods together.

5.3 Land Cover Classification Results

Total classified areas are displayed in Figure 18 and Tables 13 and 14. The total area of unobstructed channel —water, sand, and vegetation less than 2 ft in height increased in both 2018 and 2019 and returned to 2017 levels in 2020. Unvegetated channel area (water and sand) increased slightly in 2018, corresponding with losses in coverage of all vegetation classes, though primarily vegetation less than 2 ft in height. Unvegetated channel increased more substantially in 2019, likely due to the high flow events that occurred that year. Most of that increase was due to a reduction in the area of vegetation 2-6 ft in height, which decreased by approximately 50%. We infer that the increase in unobstructed area in 2019 was driven by disturbance of higher islands and near-overbank areas with tall, established vegetation.

In 2020, the coverage of vegetation 2-6 ft in height increased by over 150%, to encompass more area than was observed in 2017-2019. Water, sand, and vegetation less than 2 ft in height simultaneously decreased in coverage, suggesting that vegetation on islands and near-overbank areas recovered quickly from the 2019 flood disturbance.

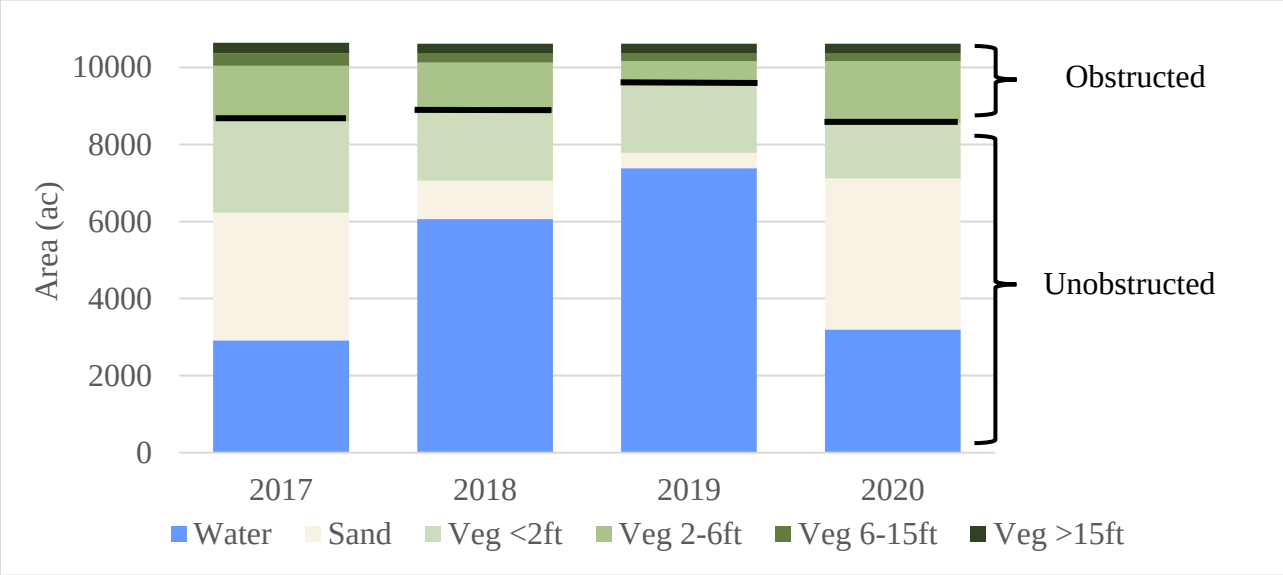

Figure 18. Total area of land cover classes in the main channel. Brackets on the right indicate classes that are grouped as obstructed or unobstructed.

Table 13. Area and % change of all classes as measured in each year in the main channel from Overton to Chapman from 2017 - 2020.

	Area (ac)				% Change		
Class	2017	2018	2019	2020	2017 - 2018	2018 - 2019	2019 - 2020
Water & Sand	6231	7060	7784	7122	13	10	-9
Veg <2ft	2373	1768	1779	1426	-26	1	-20
Veg 2-6ft	1441	1300	608	1617	-10	-53	166
Veg 6-15ft	321	232	200	192	-28	-14	-4
Veg >15ft	275	255	245	258	-7	-4	5

Table 14. Area and % change of obstructed and unobstructed main channel area in each year from Overton to Chapman from 2017 - 2020.

	Area (ac)				% Change		
Class	2017	2018	2019	2020	2017 - 2018	2018 - 2019	2019 - 2020
Unobstructed	8604	8828	9563	8548	3	8	-11
Obstructed	2037	1787	1053	2067	-12	-41	96

When plotted by river mile, MUCW (all channels) and TUCW (main channel) (Figures 19 and 20) exhibit a high degree of variability. MUCW is more variable than TUCW due to its higher sensitivity to the location of obstruction within the channel. Small in-channel obstructions can reduce MUCW by hundreds of feet, cutting it in half or more, while impacting TUCW only minimally.

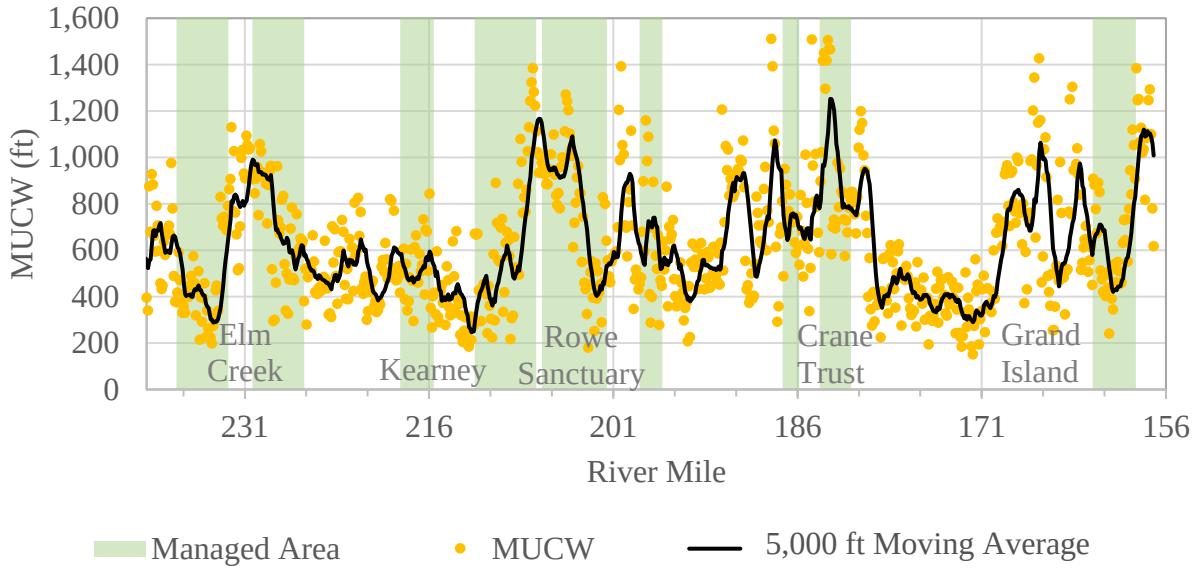

Figure 19. All channels maximum unobstructed width (MUCW), as sampled at transects spaced at 500 ft intervals, with a 5,000 ft moving average. Channel areas managed to reduce in-channel vegetation are shaded green.

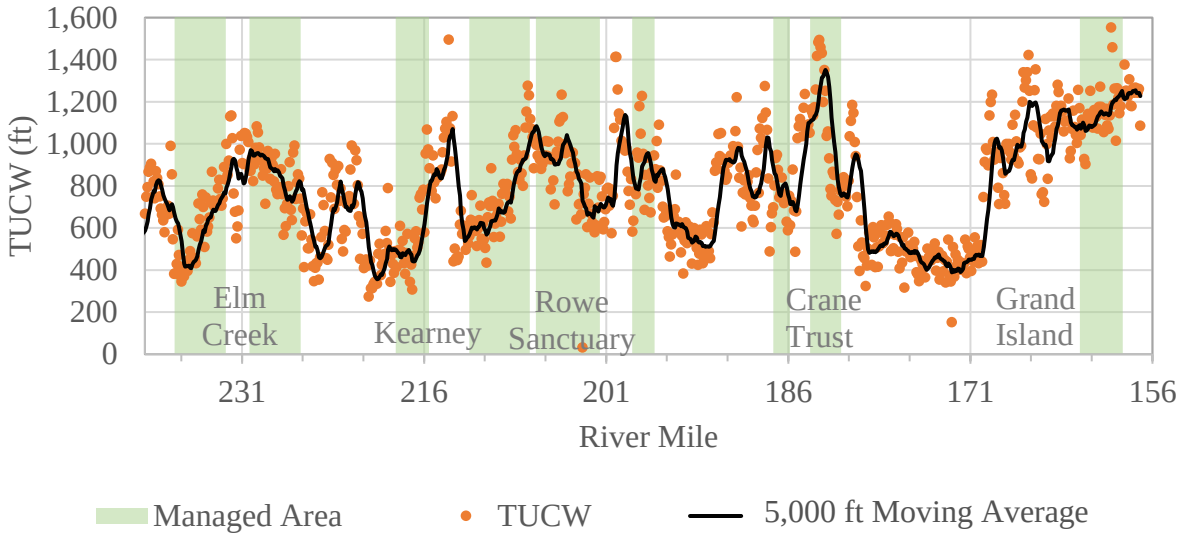

Figure 20. Main channel total unobstructed width (TUCW), as sampled at 500 ft transects, with a 5,000 ft moving average. Channel areas managed to reduce in-channel vegetation are shaded green.

When compared to the historical record of mean MUCW (all channels) and TUCW (main channel) values from visual classification (Figures 21 and 22), the period of 2017-2020 was relatively stable. The modest increase in MUCW and TUCW following the 2019 floods (<50 ft) was substantially less than the approximately 200 ft increases in both metrics that occurred in 2015.

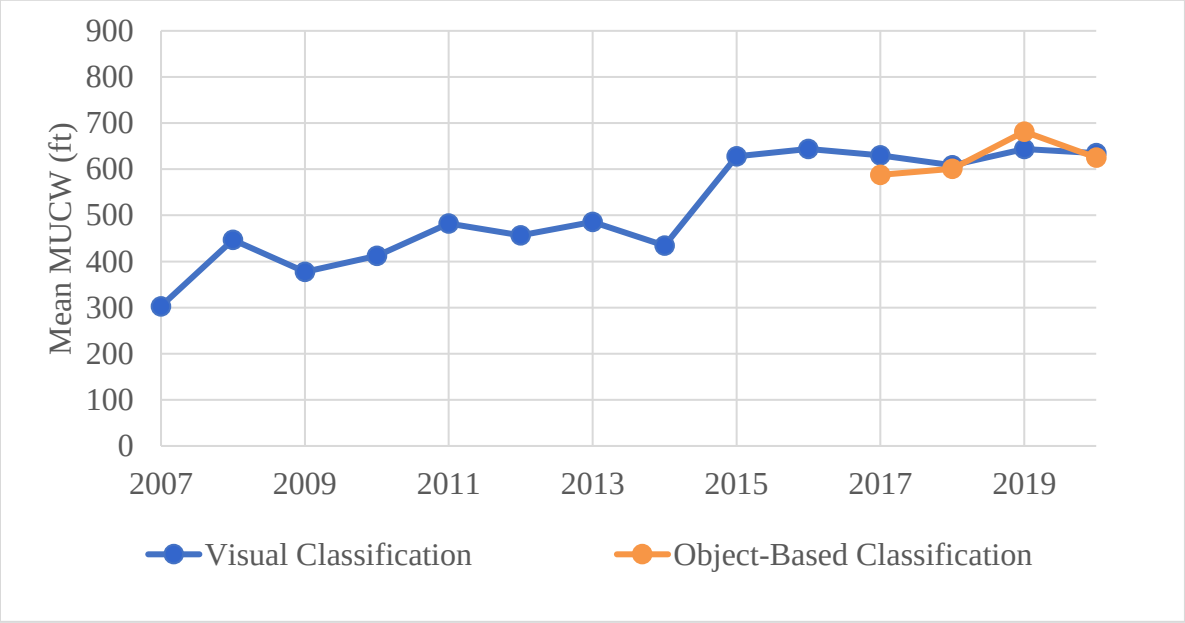

Figure 21. Mean MUCW over all channels by year from visual classification of aerial imagery and object-based classification.

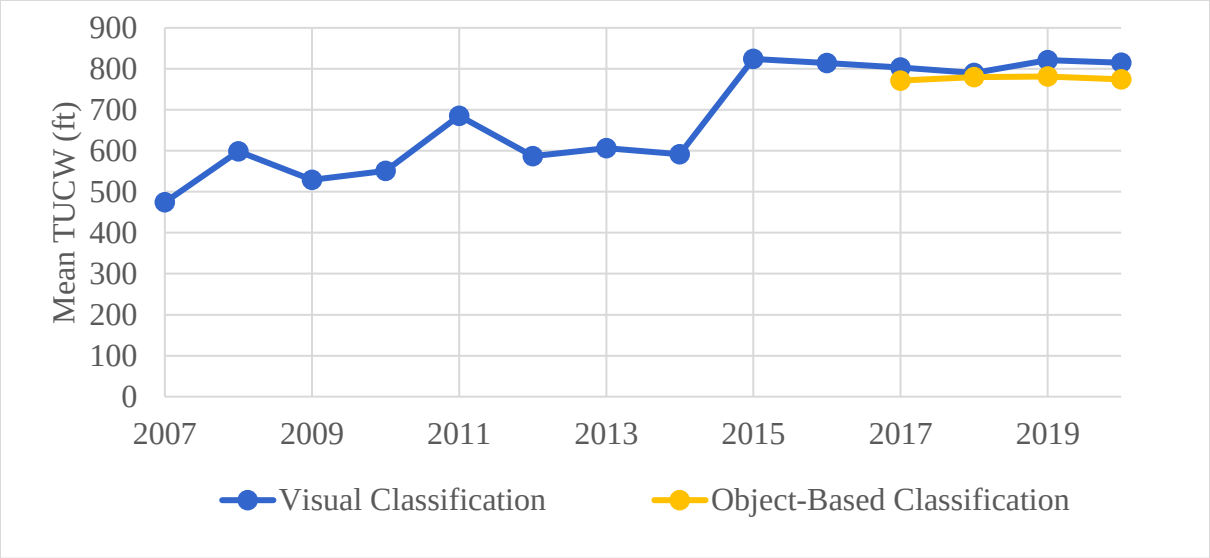

Figure 22. Mean main channel TUCW by year from visual classification of aerial imagery and object-based classification.

Prior PRRIP research indicated that mean daily peak (Q_P), 40-Day Max ($Q_{MAX\ 40}$), and mean discharge during the seed germination period in June (Q_{June}) may influence the occurrence and distribution of in-channel vegetation in the AHR (citation). These metrics are plotted together in Figure 23 with TUCW estimated from visual remote sensing from 2007-2016 and object-based classification from 2017-2020. As demonstrated in the figure, TUCW increased substantially in 2015, following a peak flow event with both high magnitude (Q_P) and duration ($Q_{MAX\ 40}$). Less substantial width responses occurred following 2008, 2011 and 2019 peak flow events. TUCW remained stable during the period of 2017-2020 despite years with no substantial peak flow. During those years, germination season flow was higher than during prior drought years (2012-2014) indicating that channel inundation during the germination season may be preventing vegetation from establishing in the channel.

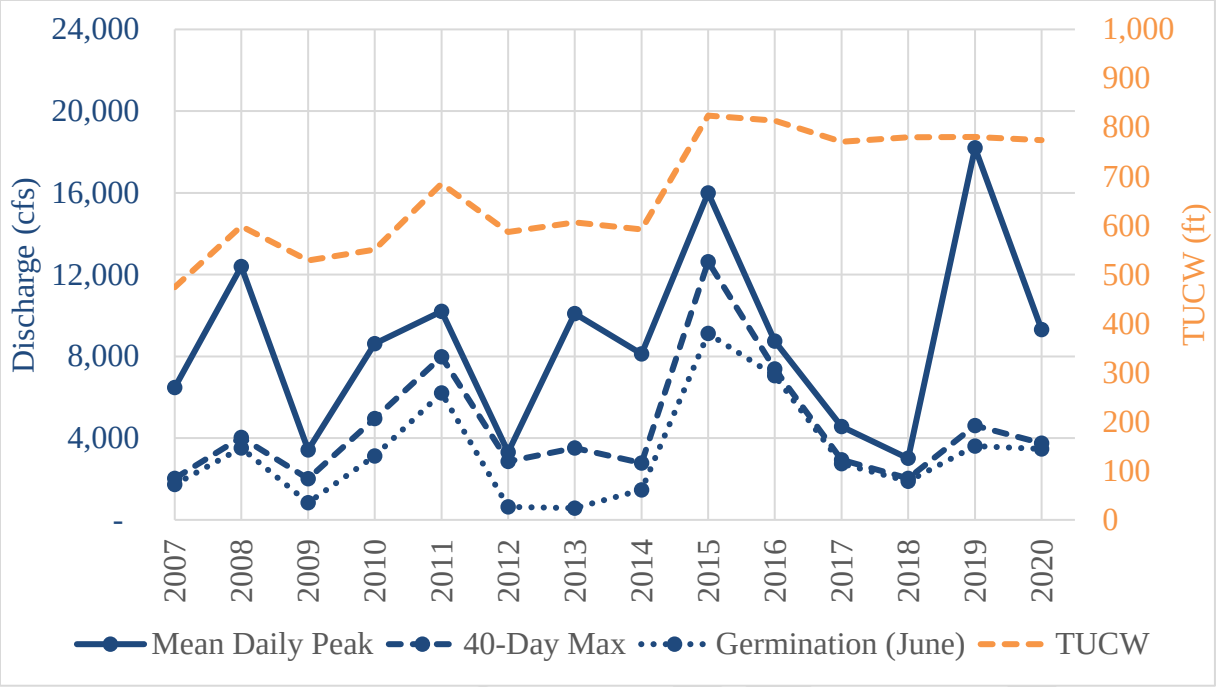

Figure 23. Hydrologic metrics and corresponding main channel TUCW as measured with visual classification from 2007 to 2020. Displayed TUCW values were estimated with visual remote sensing from 2007-2016 and object-based classification from 2017-2020.

For all years, the percent unobstructed area, MUCW (all channels), and TUCW (main channel) are all higher in areas managed by PRRIP than other areas (Figures 24- 26). Both percent channel area unobstructed and MUCW increased in both areas as a response to the 2019 floods and then returned to similar 2017-2018 levels in 2020 (Figures 24 and 25). TUCW was not evidently affected by the 2019 floods in either area (Figure 26).

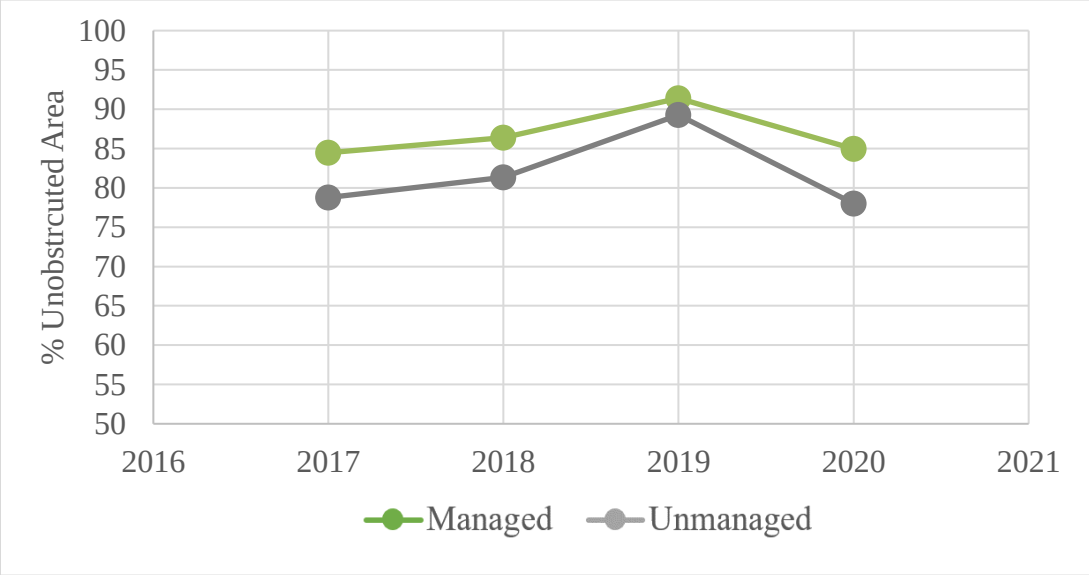

Figure 24. Percent unobstructed area in main channel areas managed to reduce in-channel vegetation (managed) and other areas (unmanaged).

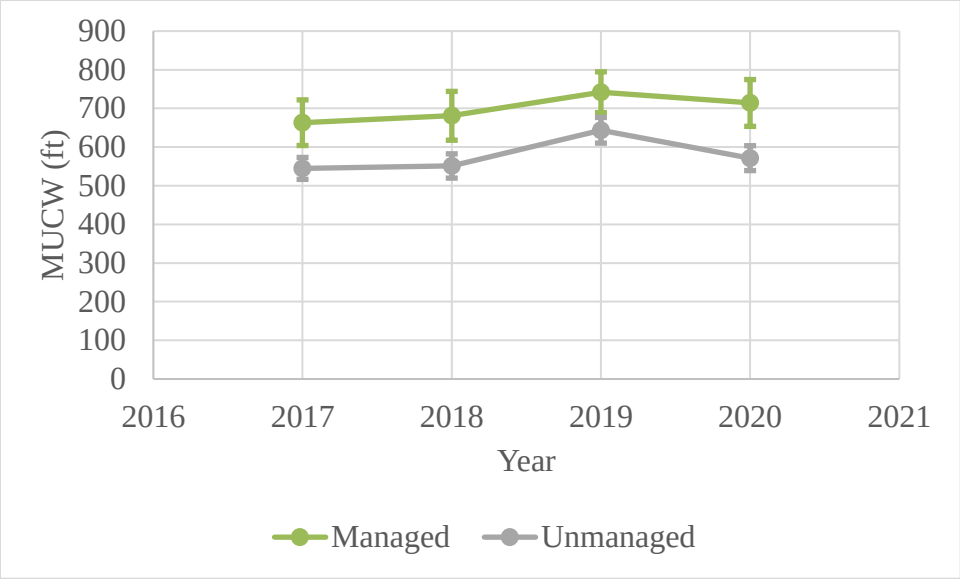

Figure 25. MUCW means (points) and standard errors (bars) of in main channel areas managed to reduce in-channel vegetation (managed) and other areas (unmanaged).

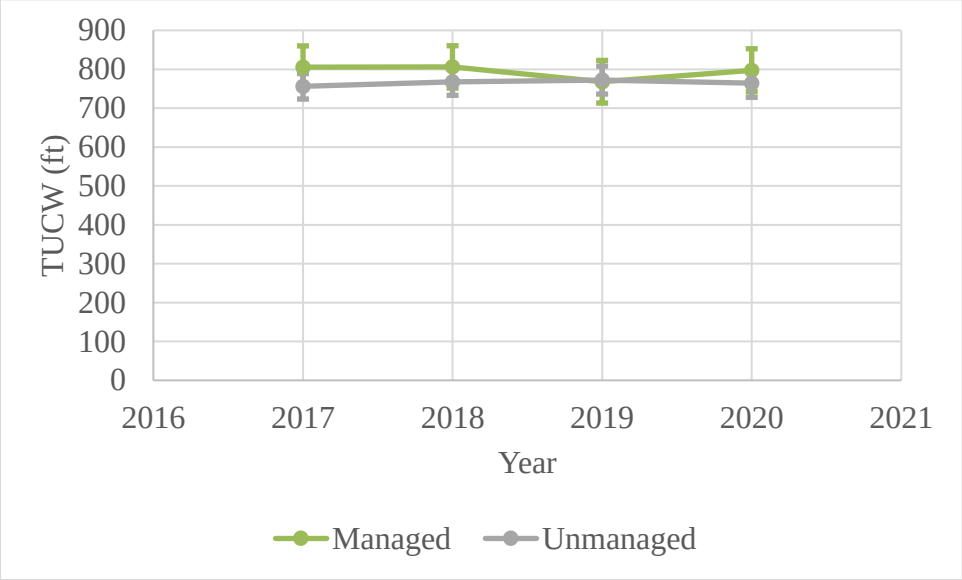

Figure 26. TUCW means (points) and standard errors (bars) in main channel areas managed to reduce in-channel vegetation (managed) and other areas (unmanaged).

A 2-sample t-test was used to understand if MUCW and TUCW of the main channel were different in managed and unmanaged areas (Table 15). A subset of transects (5,000 ft spacing) was used for comparisons to reduce spatial autocorrelation. MUCW was on average wider in managed areas, with the mean difference as much as 127 ft in 2018; however, due to high width variability between

transects, the differences were not statistically significant. TUCW values were very similar on managed and unmanaged areas, with the mean difference in all years estimated to be 10 ft or less and not statistically significant.

Table 15. Two-sample t-test results comparing main channel MUCW and TUCW values on managed vs unmanaged areas.

Year	MUCW			TUCW		
	Est. Mean Diff. Managed - Unmanaged (ft)	Diff. 95% Conf. Int.	p-value	Est. Mean Diff. Managed - Unmanaged (ft)	Diff. 95% Conf. Int.	p-value
2017	104	-28 : 237	0.12	10	-119 : 139	0.88
2018	127	-15 : 270	0.08	-8	-138 : 122	0.91
2019	94	-31 : 219	0.14	-10	-142 : 122	0.88
2020	123	-15 : 262	0.08	-4	-136 : 129	0.96

See Appendix Section E for complete land cover classification results.

6. Volume Change Analysis

Quantifying annual variation in sediment volume is critical for understanding changes in channel morphology and habitat in the AHR and for evaluating the success of management actions. A negative sediment balance resulting in a degradational channel has been identified as one of the primary drivers of historic habitat loss for the PRRIP target species (DOI, 2006).

6.1 Volume Change Methods

The 2009-2016 PRRIP field reach-wide monitoring (RWM) team collected two types of data to estimate annual sediment transport: repeat cross-section elevation surveys and repeat bed and suspended sediment load samples at five bridges. Sediment load samples were used to develop sediment transport rating curves, which were applied to annual flow data to estimate differences in sediment transport throughout the AHR. Over time, the RWM team concluded that the limited spatiotemporal coverage of samples (Tetra Tech, 2017), as well as the chaotic, episodic, and threshold-dependent nature of sediment transport (Wohl et al., 2015) limited ability to make inferences about AHR sediment dynamics based on the field-based RWM protocol.

An alternative to collecting field-based data is to use LiDAR or other remote sensing tools to create digital elevation models (DEMs) of the complete region of interest. The newer DEM elevation values are subtracted from the older values, yielding a DEM of Difference (DoD). The DoD values can be summed together to directly estimate the net bed volume change. DoD values can also be analyzed spatially to determine where aggradation or degradation occurs within a reach, and at what magnitude. The updated RWM protocol utilizes this method based on topobathymetric LiDAR data. Due to the fundamental differences in sampling method and spatial coverage between the field and remote sensing methods, the PRRIP Independent Science Advisory Committee

(ISAC) recommended that field-based volume change estimates not be used in tandem with the remote sensing-based estimates in this or future analyses (PRRIP, 2022).

The LiDAR elevation data were collected from an airplane by QSI in either October or November of the years 2016-2020. The rasters have 3 ft spatial resolution and vertical error of less than 3 inches for dry areas and less than or equal to 9 inches for wet areas (QSI, 2016; QSI, 2017; QSI, 2018; QSI, 2019; QSI, 2020). All accuracy values are presented in Table 16. Accuracy was assessed by QSI at the time of data collection, and is based on comparison of field RTK GPS ground control check points to the LiDAR DEM. The accuracy values represent the 95% confidence interval, as derived from the population of differences between field-measured and DEM values. QSI's accuracy assessments are designed to meet the guidelines of the Federal Geographic Data Committee National Standard for Spatial Data Accuracy (FGDC, 1998). The accuracy assessment data indicate elevation values in wet areas had consistently higher uncertainty than dry areas across all years. As a result of deeper and more turbid water during the period of data collection, wet areas in 2019 had a higher uncertainty value at 9 inches (Table 16).

Table 16. Accuracy estimates for the LiDAR DEM surfaces from each year for wet and dry areas. Accuracy values represent 95% confidence in the estimate.

Year	Dry Accuracy (in)	Wet Accuracy (in)
2016	1.7	3.1
2017	2.2	4.6
2018	1.2	4.2
2019	1.2	9.0
2020	2.2	3.1

The software Geomorphic Change Detection 7.5 (GCD) from the Riverscapes Consortium (Riverscapes Consortium, 2020) was used for most components of the volume change analysis. GCD is a GIS-based software designed to estimate sediment budgets via the morphological method and quantify associated error. A conceptual model representing the processing is given in Figure 27.

Estimating error is a critical component of volume change analysis. Each DEM has its own error which is then propagated through to the DoD. Several methods exist in the literature for quantifying error from DoD-derived sediment budgets. Recent research (e.g. Wheaton et al., 2010; Bangen et al., 2016) has suggested that for many rivers, error is not spatially uniform, but varies considerably with conditions of the surface like roughness, slope, and vegetation. In this case, fuzzy inference systems (FIS) may serve as a good framework to quantify spatially variable error (Wheaton et al., 2010). Examining the elevation distribution of coincident points, or LiDAR points that are within a negligible XY distance from each other, has been proposed as a method to examine the spatial distribution of error and develop boundaries for FIS groups (Hensleigh, 2014).

A preliminary analysis of coincident points in a sample reach for one analysis year was completed to examine the effect of slope, water depth, and vegetation height on the elevation difference of

coincident points (serving as a proxy for error). None of the factors were found to have a significant effect on proxy error. This is likely due to the consistently low values of slope, water depth, and grain size on the Central Platte. Therefore, a FIS-based spatially variable error model was not used for this analysis.

Instead, error was assumed to be spatially constant within wet and dry areas, but different between them, based on the QSI accuracy estimates presented in Table 16. Following differencing of the elevation values to produce a DoD, each difference value was assigned a probability that the change was real, rather than a result of measurement error, based on a combination of the difference magnitude and uncertainty associated with the two differenced DEMs. The difference values were then thresholded probabilistically at 95%, consistent with the Lane et al. (2003) method. The result of this method was that elevation differences falling below the confidence limit were excluded from the volume change calculation. Significant elevation differences (exceeding the confidence limit) were summed to yield the net volume change for each reach and analysis year.

For each area of interest over which difference values were summed to yield volume change, the error of the volume change estimate was calculated as the sum of the propagated elevation uncertainty values across the DoD surface, multiplied by area, consistent with Lane et al. (2003). These error values were used to evaluate the significance of volume change estimates. If volume change confidence interval was below 0, the area was determined to be significantly degradational, meaning that it experienced a net loss of sediment during the time period. If the confidence interval was above 0, the area was determined to be significantly aggradational. If the confidence interval crossed 0, it was not possible to determine with confidence whether the area was aggradational or degradational.

This remote sensing method also allows for the elevation differences of each cell to be classified, and both the area and volume change separated by class. The elevation difference (ΔZ) classifications used in this analysis are as follows:

1. Aggradation
2. Bed degradation
3. Lateral Erosion

Aggradation and bed degradation represent low-magnitude positive and negative elevation differences typically associated with the migration of sandbars. An area with bed degradation that outpaces aggradation may be incising. Lateral erosion represents large-scale negative elevation changes near the channel banks and on the margins of established islands. High levels of lateral erosion are an indication of channel widening. For this analysis, lateral erosion areas were classified as areas along channel/bar/island margins (within 20 ft of the modeled 5,000 cfs flow extent) with an elevation difference less than or equal to -2 ft. Areas of bed degradation were classified as all remaining significantly negative areas.

Net bed volume change was subsequently calculated by subtracting the magnitude of bed degradation from aggradation. Lateral erosion is not included in the net bed volume change calculation, because it is a measure of channel bank change rather than channel bed change.

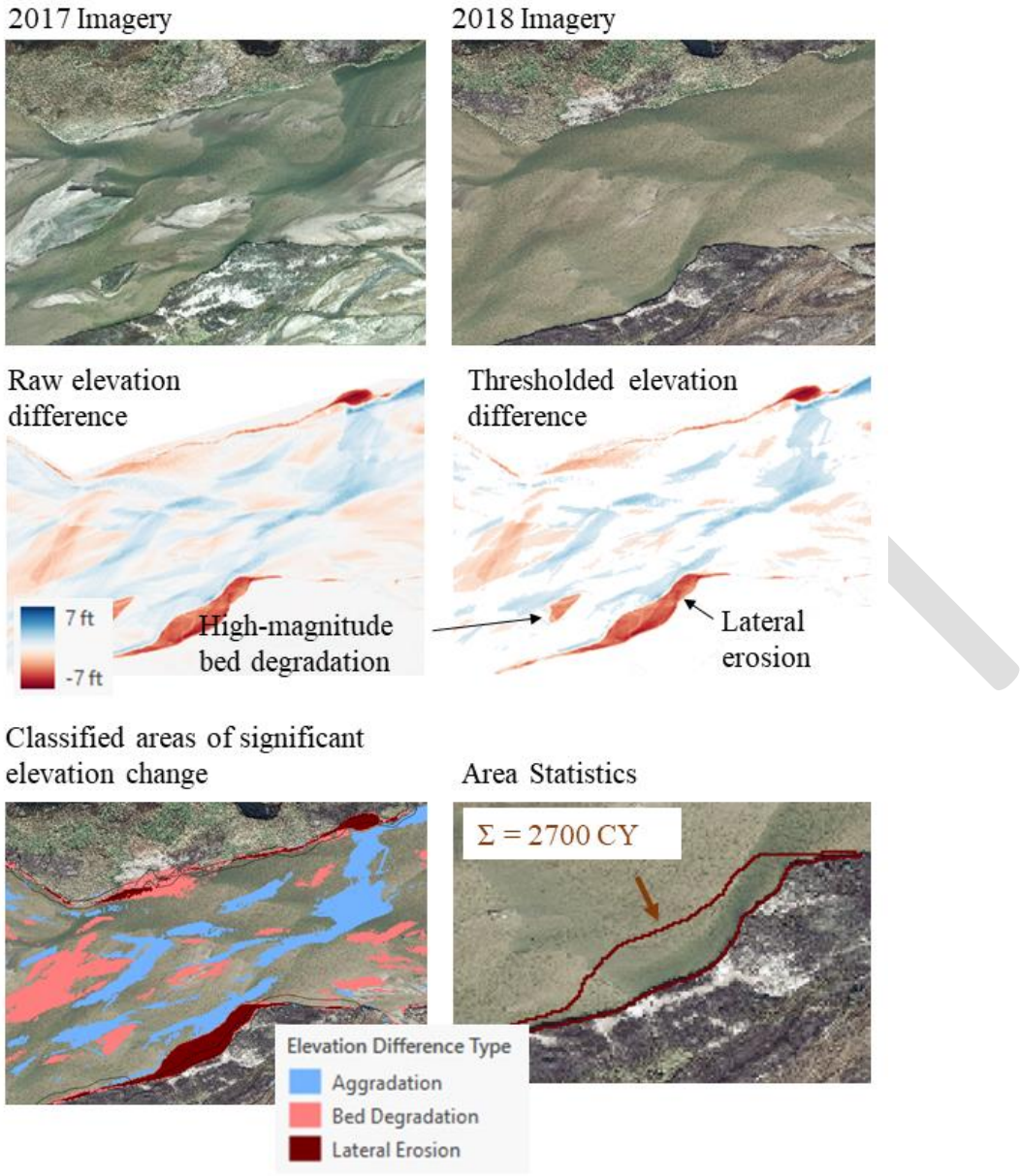

Figure 27. Conceptual diagram outlining how elevation values of two years are differenced, thresholded based on probability, classified by difference type, and analyzed spatially.

The lateral erosion estimate was adjusted for the J2 Return to Overton reach to account for sediment augmentation activities in the reach. The analysis mask included the area excavated for the purposes of sediment augmentation, and the classification algorithm automatically classified the excavation area as lateral erosion. The volume of excavated material is quantified annually for sediment augmentation monitoring and is reported to the U.S. Army Corps of Engineers. Excavation volume is quantified by differencing the fall and summer LiDAR elevations for the excavation area within the same year. Lateral erosion and sediment augmentation volume are presented separately for the J2 Return to Overton reach.

6.3 Volume Change Results

The AHR net sediment balance analysis indicates that 2017-2020 was a period of relative stability (Figure 28). The net volume change estimates were negative for all analysis years except 2019-2018, though the confidence interval for all years crossed 0, indicating that no year in this period was either significantly net aggradational or degradational.

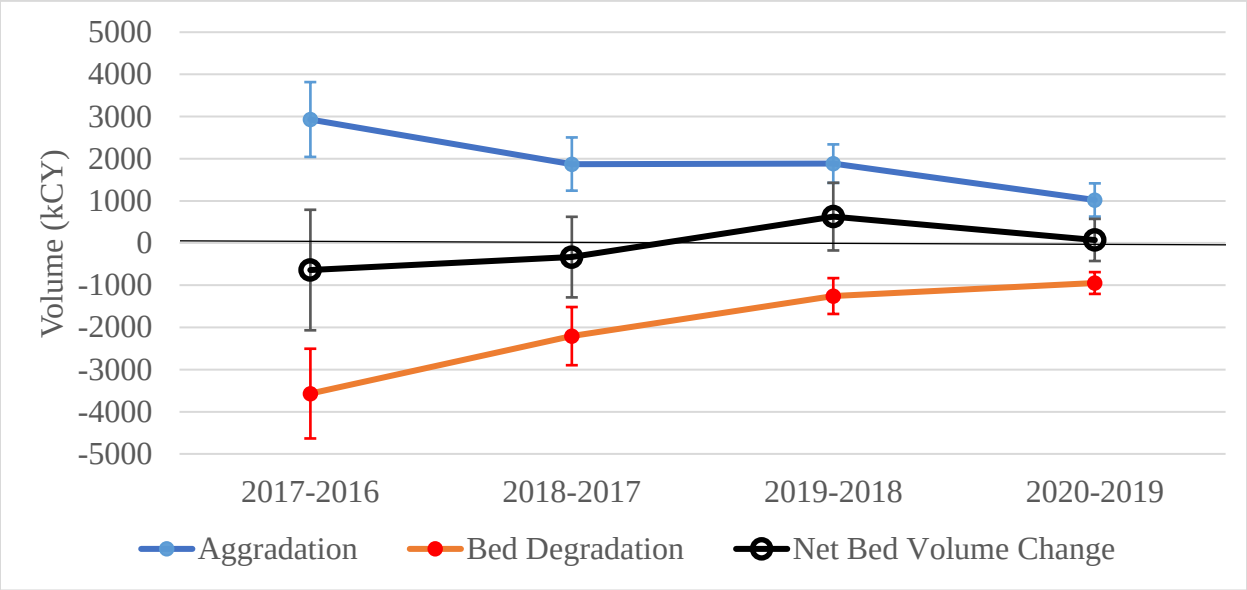

Figure 28. Total volumes of significant elevation change (points), and error (bars), classified as either aggradation or bed degradation, with net bed volume change, for all channels from Overton to Chapman.

When making sediment balance comparisons between years, it is important to note that the higher uncertainty values in wet areas in 2019 reduced the total area that met the significance threshold necessary for inclusion in the analysis. Nevertheless, a signature from the 2019 floods is evident when significant elevation differences are classified (Figures 28 - 30). 2019 saw an increase in both the area of aggradation (Figure 29) and the volume of lateral erosion (Figure 30). Bed degradation did not increase in 2019 in correspondence with the rate of aggradation. This indicates that the dominant sediment dynamic during the floods was lateral erosion and subsequent deposition of eroded material, rather than general bed erosion. The elevated magnitude of lateral erosion volume in 2019 (Figure 30) suggests that certain areas of the channel experienced widening. This is reflected in a slight (non-significant) increase in wetted width at the AHR-scale (Figure 8).

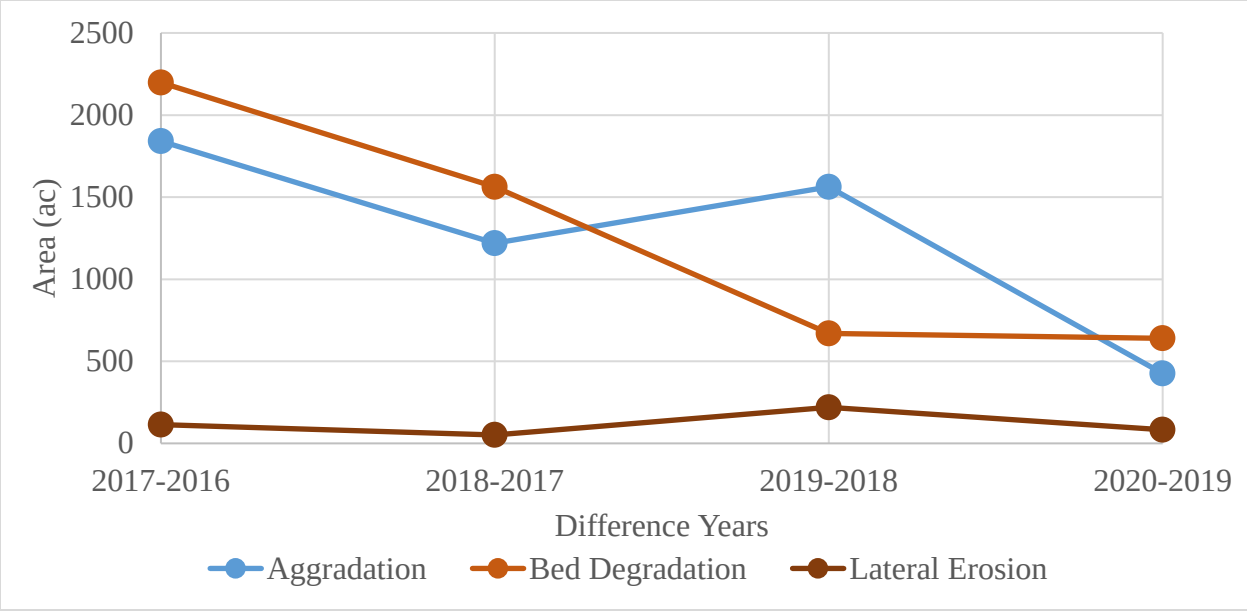

Figure 29. Total area of significant elevation change classified as either aggradation, bed degradation, or lateral erosion between years. These values represent all channels from Overton to Chapman.

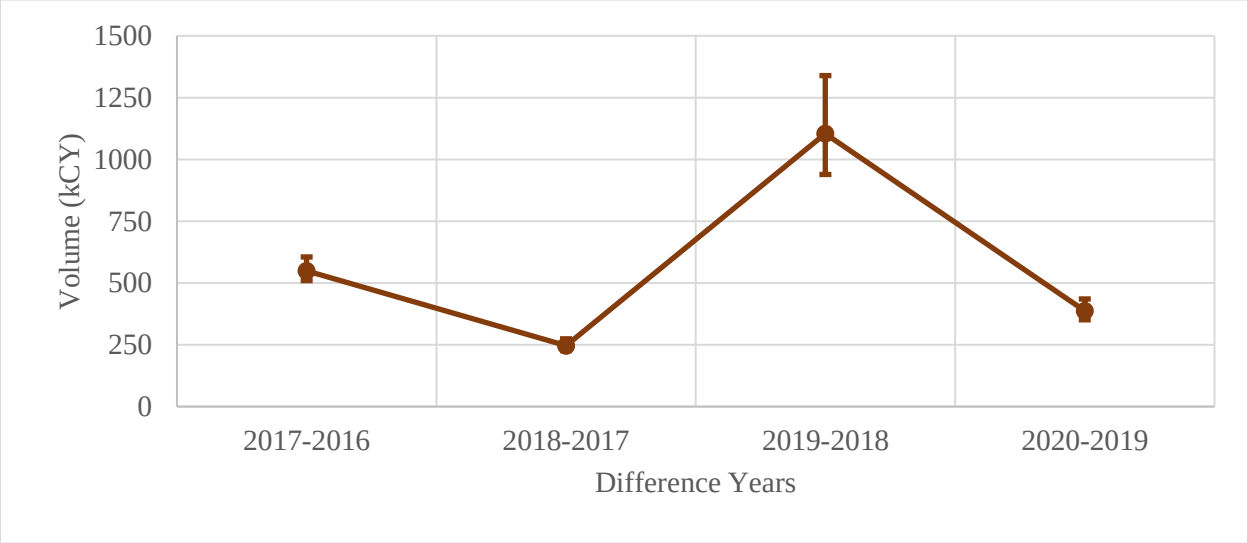

Figure 30. Total volume of lateral erosion (points) with estimated error (bars) by year. These values represent all channels from Overton to Chapman.

While the net bed volume change estimate for all reaches from Overton to Chapman was positive, but not significantly positive for the 2019-2018 analysis (Figure 28), many individual reaches were significantly aggradational during that time period (Figure 31). The 5 reaches from Odessa to Chapman, as well as the north channel from Lexington to Overton, all experienced a net gain in channel bed volume. The aggradation may reflect material that was laterally eroded during the 2019 floods and subsequently deposited in the channel bed.

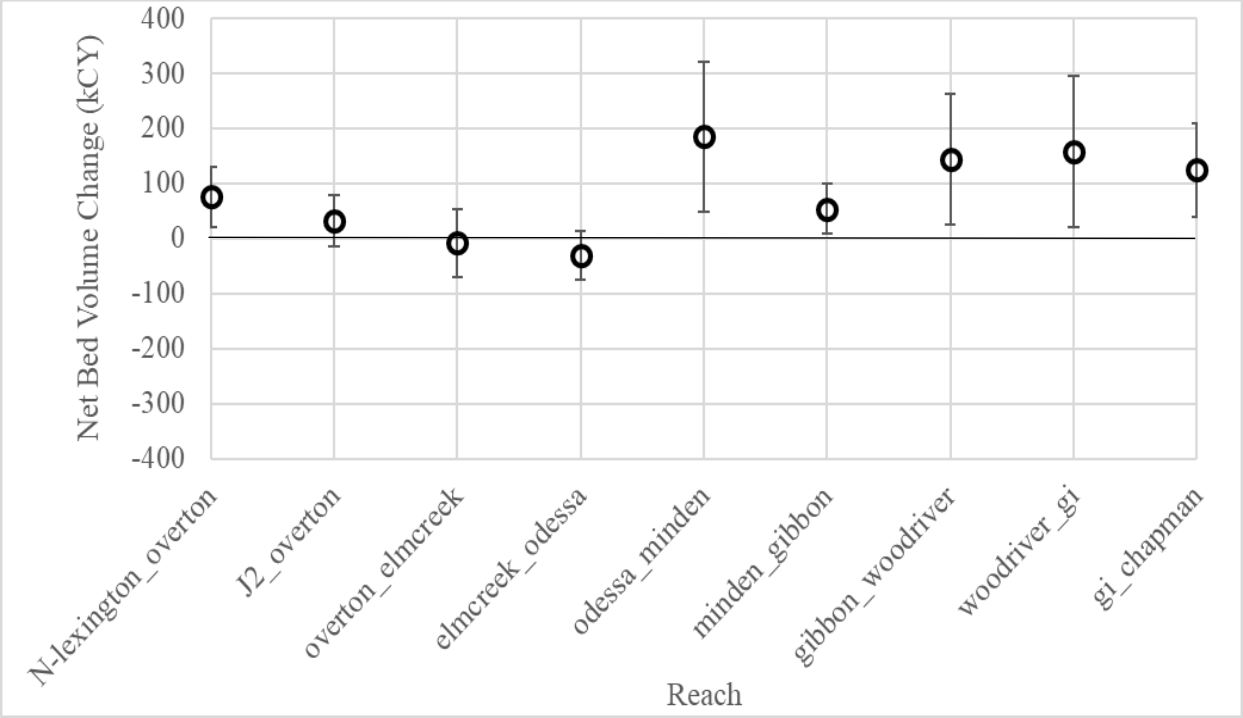

Figure 31. Net channel bed volume change estimates (points) and estimated error (bars) for all channels by reach, 2019-2018.

The geomorphic reaches from Overton to Chapman have similar rates of lateral erosion when averaged by river mile (Figure 32). However, the north channel from Lexington to Overton has notably lower values of lateral erosion than the other reaches, while the J2 Return to Overton reach experienced significantly higher rates of lateral erosion than all other reaches. The data represented in Figure 32 are only for one difference surface—2019-2018—however, the pattern was consistent across all years examined. The north channel from Lexington to Overton likely has lower rates of lateral erosion because of consistently lower flow in that channel relative to others below the J2 Return, as well as the dominance of tall, woody vegetation in that reach, which stabilizes banks.

Sediment augmentation volume is included in addition to lateral erosion for the J2 Return to Overton reach in Figure 32. Lateral erosion and sediment augmentation may play similar roles in channel sediment dynamics by introducing material to the channel bed.

The high rate of lateral erosion in the J2 Return to Overton reach is likely due to a combination of reach slope and hydrology, which is dominated by the clearwater hydropower return flows from the J2 Canal. Sediment-starved water entering the channel at the J2 Return has resulted in high rates of bed degradation in the reach, which has in turn reduced channel slope. Much of the upper portion of the reach with reduced slope has transitioned from a braided planform to a single-thread wandering planform that meanders back and forth across the incised channel section, laterally eroding floodplain terraces along the outside of bends.

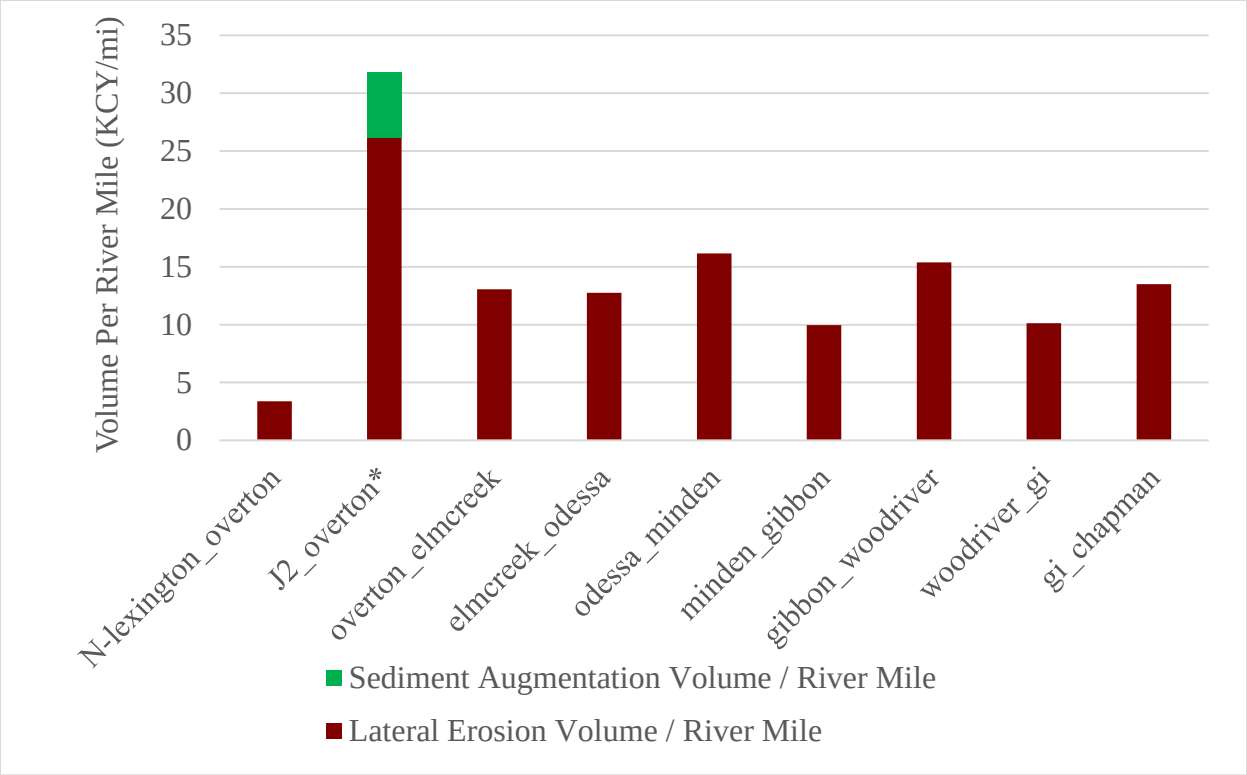

Figure 32. Lateral erosion volume by geomorphic reach for all channels for the analysis period 2019-2018. **Sediment augmentation in the J2 Return to Overton reach is subtracted from the classified lateral erosion volume, and reported separately.*

The sediment balance of the J2 Return to Overton reach is of particular interest to PRRIP. The reach has a history of incision and narrowing because of the sediment-starved water entering the river at the return. PRRIP sediment augmentation efforts have been focused on this reach since 2017 to halt the downstream progression of incision and narrowing. 6 KCY / river mile of sediment was mechanically augmented to the J2 Return to Overton reach in 2019 (Fig. 32). Additionally, 26 KCY / river mile of sediment was laterally eroded within the reach (Fig. 32). Lateral erosion may act as a natural sediment augmentation by adding sediment to the channel bed within the reach and downstream.

Volume change and net sediment balance of the J2 Return to Overton reach are presented in Figure 33. The reach had a positive, though not significant, net channel bed volume difference for 3 out of 4 analysis years (Figure 33). The sediment balance within the reach is not an adequate measure of success of sediment augmentation efforts, which are targeted primarily to address habitat areas downstream like Cottonwood Ranch. To address this question directly, volume differencing data such as these will be incorporated into a systematic and streamlined approach to measure the success of sediment augmentation by the EDO in 2022.

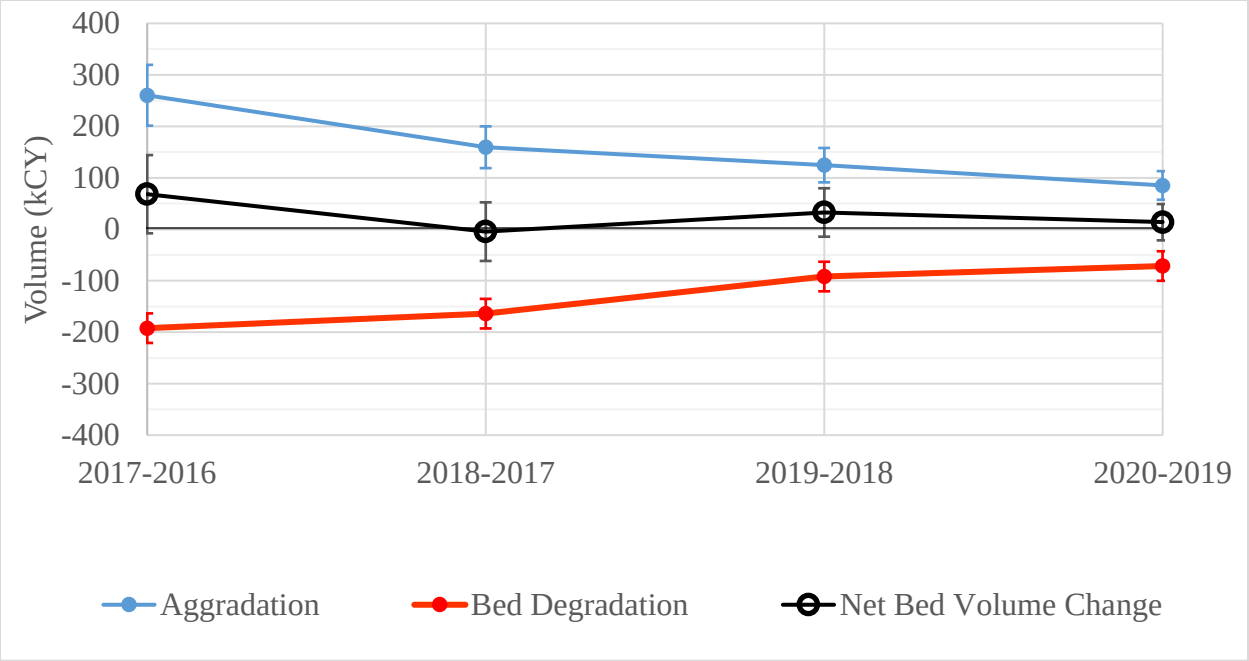

Figure 33. Total volumes of significant elevation change (points), and error (bars), classified as either aggradation or bed degradation, with net bed volume change, for the J2 Return to Overton reach.

See Appendix Section E for complete volume change analysis results.

7. Suitable Whooping Crane Roosting Habitat

7.1 Suitable Whooping Crane Roosting Habitat Methods

Suitable WC roosting area is defined here as an area of channel with unobstructed width wider than 650 ft and depth shallower than 1 ft. These criteria were determined through analysis of whooping crane telemetry data by Pearse et al. (2016) and Baasch et al. (2019). The area of suitable roosting habitat has been evaluated by intersecting unobstructed width results from the land cover classification and depth results from the hydrodynamic modeling (Figure 34).

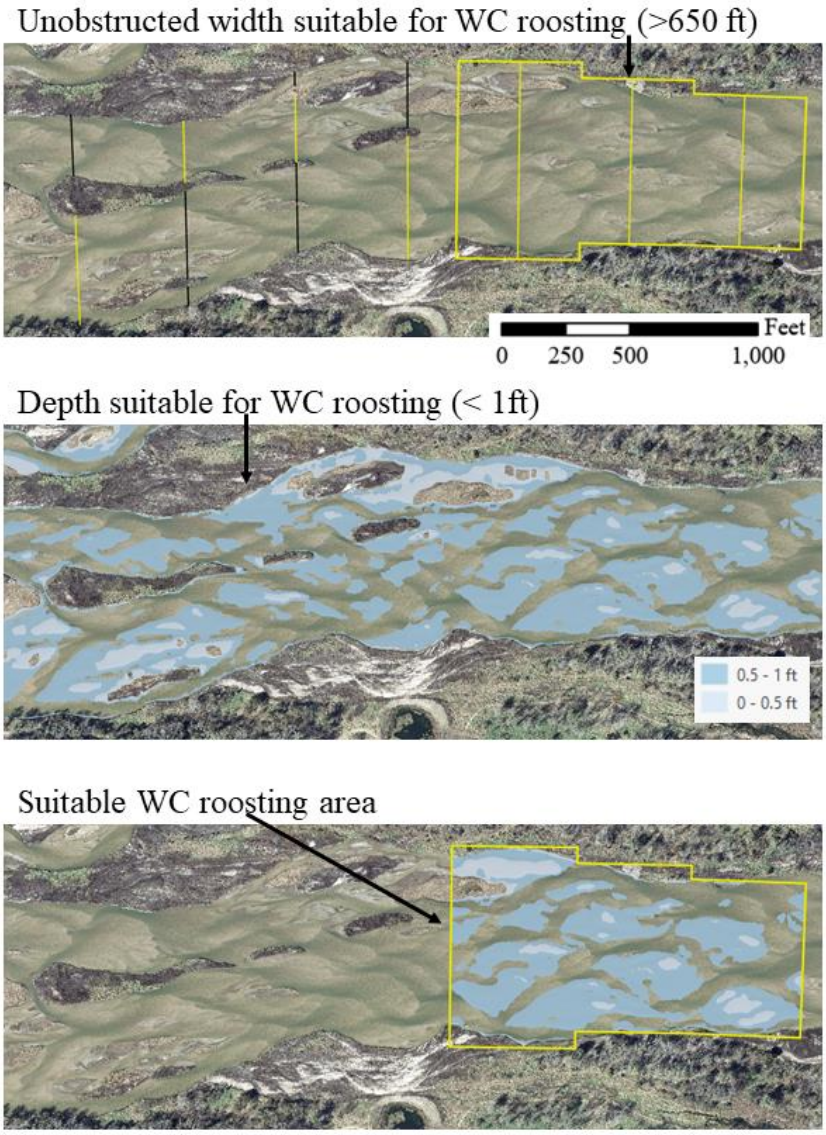

Figure 34. Conceptual diagram illustrating the classification of suitable WC roosting area by intersecting unobstructed width and modeled depth results.

7.2 Suitable Whooping Crane Roosting Habitat Results

Due to its dependence on the availability of suitably shallow water, the area of suitable roosting habitat in the AHR is maximized at a flow of approximately 750 cfs (Figure 35). The area of suitable roosting habitat on the main channel is considerably greater in the geomorphic segments from Minden to Chapman due in part to longer reach length (Figure 36). When considered as an area percentage, the reaches Elm Creek to Odessa, Gibbon to Wood River, Wood River to Grand Island, and Grand Island to Chapman have similar values for percent suitable roosting area, ranging from 21-31%. Overton to Elm Creek and Odessa to Minden have lower values, at 10 and 7%, respectively. The Minden to Gibbon reach stands out with 73% suitable whooping crane roosting area at 2000 cfs.

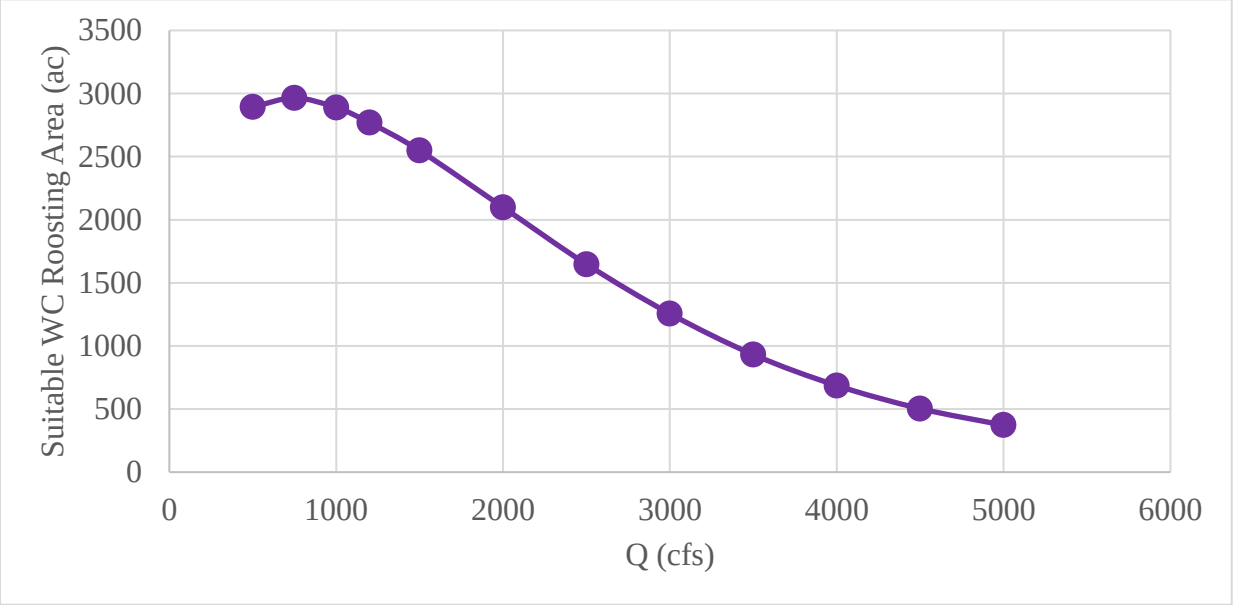

Figure 35. Suitable whooping crane roosting area in the AHR by modeled flow, for all channels in 2020.

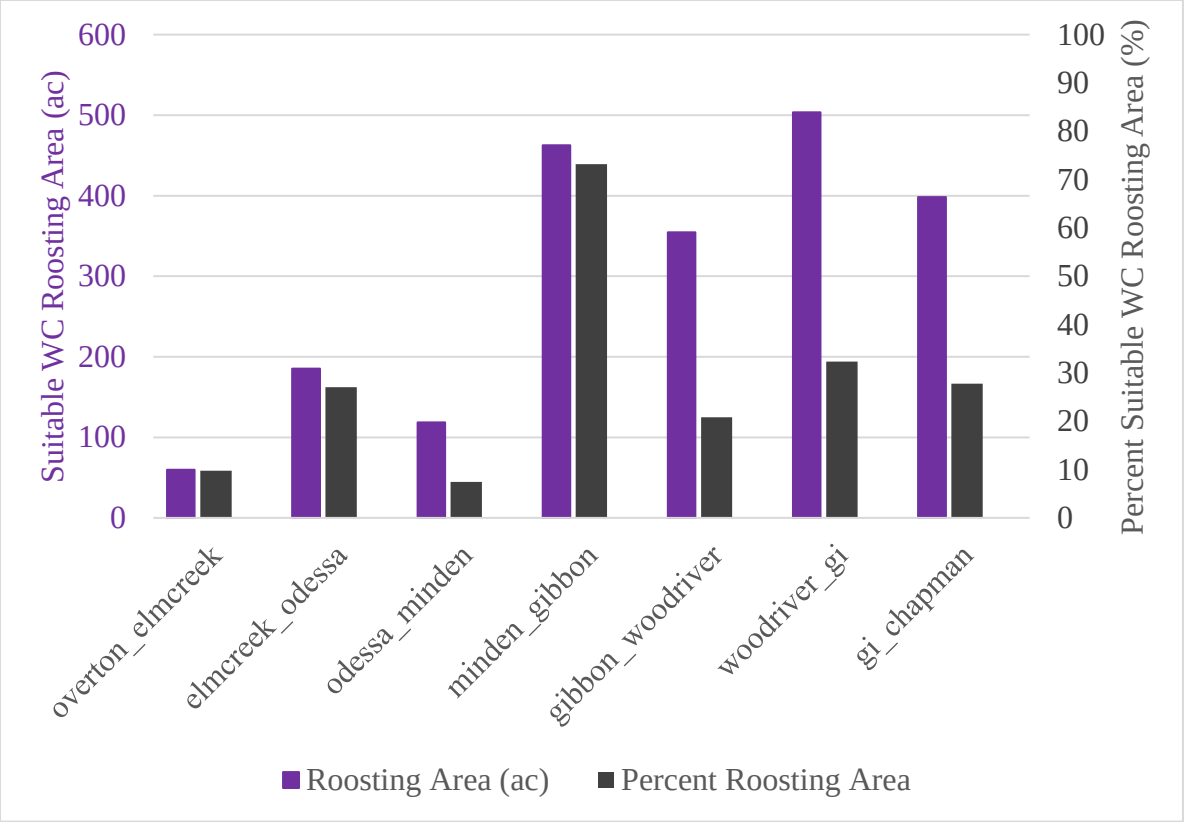

Figure 36. Absolute and percent suitable roosting area by geomorphic reach for the main channel, modeled at 2000 cfs with 2020 data.

Managed lands have consistently higher percent whooping crane roosting area values than other main channel areas across all years (Figure 37). Both areas experienced an increase in the availability of suitable roosting habitat in 2019, likely as a response to the floods. Both areas also saw a return to similar 2017-2018 levels in 2020. The temporal trend more closely mirrors the trend in MUCW (Figure 21) than the area with depth less than 1 ft (Figure 12), suggesting that the 2019 flood impacts of roosting habitat availability were driven by change in vegetation cover rather than change in depth.

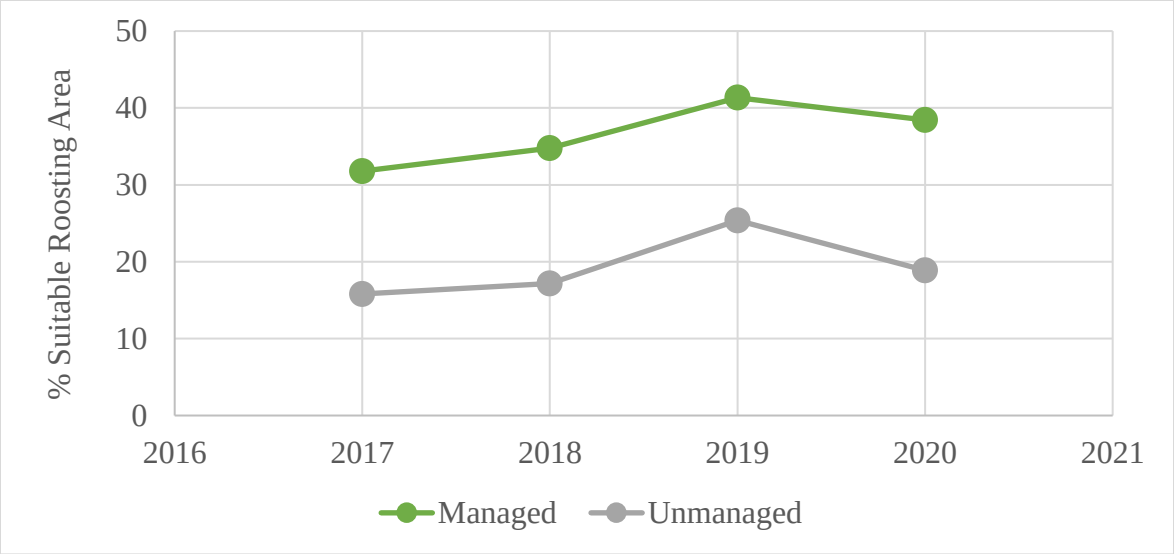

Figure 37. Percent suitable roosting area at 2000 cfs over time for managed areas vs. unmanaged areas of the main channel.

See Appendix Section G for complete suitable whooping crane roosting area results.

8. Emerging Issues

Over the course of the last several years, the EDO noted that the main channel along the southern edge of Mormon Island (Wood River to Grand Island reach) was becoming increasingly vegetated and the middle channel through the island was simultaneously widening. A review of aerial imagery indicates a substantial shift in the flow split at that location through time (Figure 38). In 2001, south (main) channel width at the split was 460 ft and middle channel width at the split was 265 ft. By 2020, the middle channel was wider (350 ft) than the south channel (340 ft).

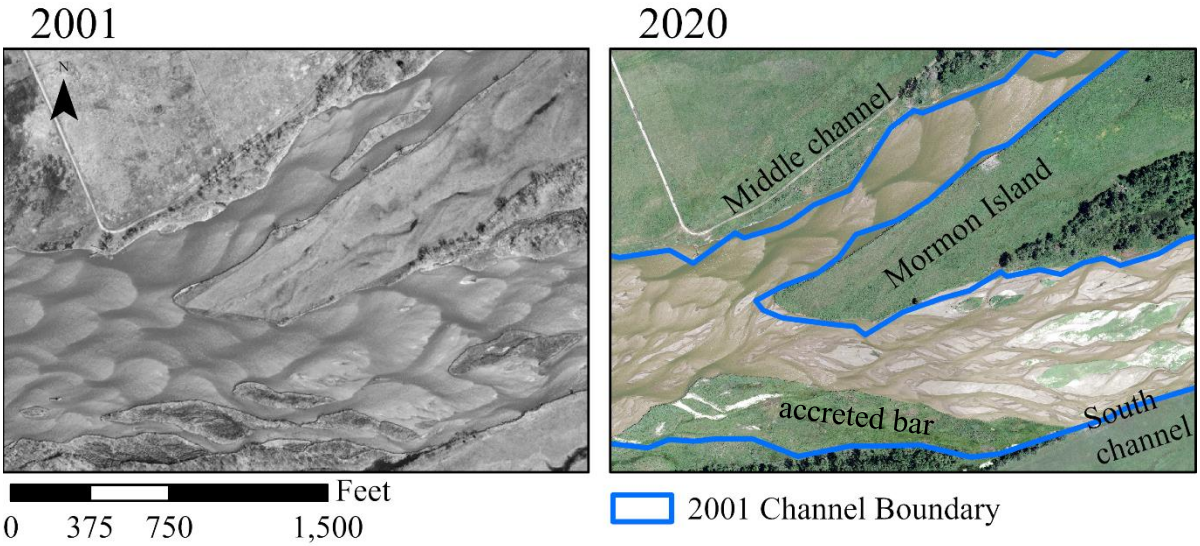

Figure 38. Aerial imagery from 2001 and 2020 in the vicinity of Mormon Island. A polygon representing the 2001 channel extent is overlain on the 2020 imagery.

We utilized the 2017-2020 hydrodynamic models to evaluate split flow at that location at 500 and 2,000 cfs (Table 17). Figure 39 presents the modeled distribution of depths at 2,000 cfs. As demonstrated in the table and figure, more than half of the flow is now conveyed by the middle channel with substantially less flow and correspondingly shallower flow depth occurring in the south channel. In 2020, an estimated 25% of main channel flow was conveyed by the south channel at 2,000 cfs.

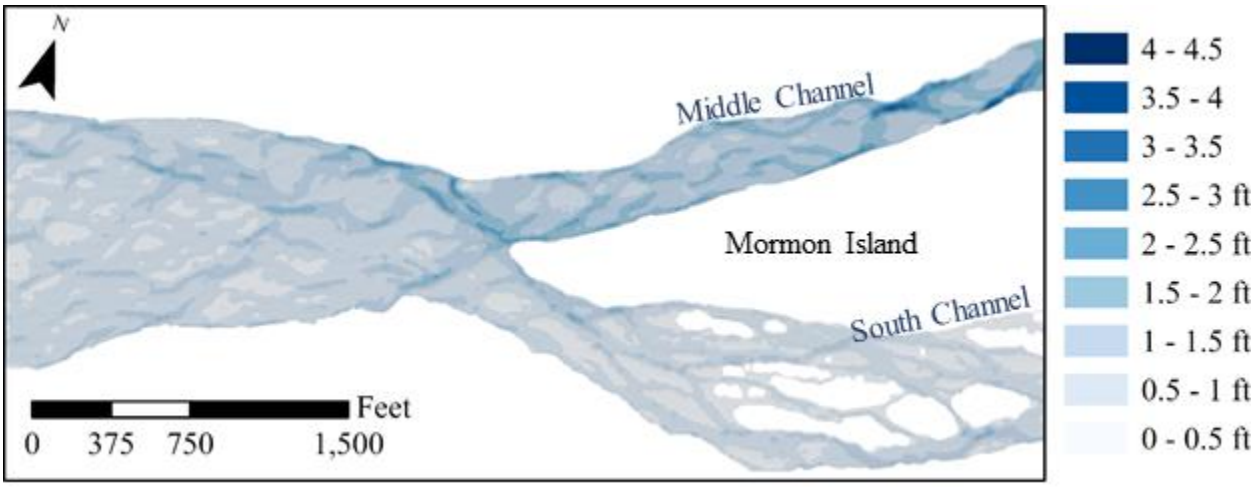

Figure 39. Model flow depths (2020) at 2,000 cfs. Flow is substantially deeper in the middle channel than the south channel, which historically carried the majority of flow around the south side of Mormon Island.

Table 17. Mormon Island flow split (2020 model) at 500 and 2000 cfs.

	% Flow in South Channel			
Q (cfs)	2017	2018	2019	2020
500	17	14	24	12
2000	30	29	33	25

This shift in flow distribution has likely been caused by the accretion of a large bar along the south bank at the upstream end of the south channel (Figure 38). This flow obstruction directs flow toward the middle channel at low and moderate discharges. Over time, we expect WC habitat suitability to decline in the 11-mile segment of the south channel downstream of the flow split as the previously highly suitable channel vegetates and narrows. At the same time, middle channel suitability is expected to increase as that channel widens, although at 350 ft, it is much narrower than the 650 ft MUCW that the Program considers to be highly suitable for WC roosting. Mechanical vegetation control in the south channel will slow the rate of decline in suitability but will requiring increasing effort over time.

9. Big Questions

The Program's First Increment Extension Science Plan will be finalized in early 2022. The 2022 System-scale Geomorphology and Vegetation Monitoring Report will include a section relating monitoring results to Extension big questions.

10. References

Aquaveo, 2010. Surface-water Modeling System. Online Users Manual. https://www.xmswiki.com/wiki/Main_Page

Baasch, D.M., Farrell, P.D., Howlin, S., Pearse, A.T., Farnsworth, J.M. & Smith, C.B., 2019. Whooping crane use of riverine stopover sites. PloS ONE 14(1).

Bankhead, N., 2012. Directed Vegetation Research: Lateral Bar Erosion Study. Platte River ' Recovery Implementation Program.

Bangen, S., Hensleigh, J., McHugh, P., & Wheaton, J., 2016. Error modeling of DEMS from topographic surveys of rivers using fuzzy inference systems. Water Resources Research, 52.

Blaschke, T., 2010. Object based image analysis for remote sensing. ISPRS Journal of Photogrammetry and Remote Sensing 65, 2-16.

Bureau of Reclamation, 2008. SRH-2D version 2: Theory and User's Manual: Sedimentation and River Hydraulics—Two-Dimensional River Flow Modeling.

Burnett, C. & Blaschke, T., 2003. A multi-scale segmentation/object relationship modelling methodology for landscape analysis. Ecological Modeling 168, 233-249.

Demarchi, L., Bizzi, S. & Piegay, H., 2016. Hierarchical Object-Based Mapping of Riverscape Units and in-Stream Mesohabitats using LIDAR and VHR Imagery. Remote Sensing 8, 97.

Department of the Interior (DOI), 2006. Biological Opinion on the Platte River Recovery Implementation Program.

Fansworth, J.M., Baasch, D.M., Farrell, P.D., Smith, C.B., & Werbylo, K.L., 2018. Investigating whooping crane habitat in relation to hydrology, channel morphology and a water-centric management strategy on the central Platte River, Nebraska. Heliyon, 4(10).

Federal Geographic Data Committee (FGDC), 1998. Geospatial Positioning Accuracy Standards, Part 2: Standard for Geodetic Networks. FGDC-STD-007.2-1998

Fotherby, L.M., 2009. Valley confinement as a factor of braided river pattern for the Platte River. Geomorphology, 103(4).

Hensleigh, J., 2013. Geomorphic Change Detection Using Multi-beam SONAR. [Master's thesis, Utah State University]. DigitalCommons@USU.

Interagency Advisory Committee on Water Data, 1982. Guidelines for determining flood flow

frequency. Bulletin 17B of the Hydrology Subcommittee, Office of Water Data Coordination, U.S. Geological Survey (USGS).

Lane, S.N., Westaway, R.M. & Hicks, M., 2003. Estimation of erosion and deposition volumes in a large, gravel-bed, braided river using synoptic remote sensing. Earth Surface Processes and Landforms, 28.

McFeeters, S.K., 1996. The use of the Normalized Difference Water Index (NDWI) in the delineation of open water features. Remote Sensing Letters 17(7).

Murphy, P.J., Randle, T.J., Fotherby, L.M., Daraio, J.A., 2004. The Platte River Channel: History and Restoration. U.S. Department of the Interior, Bureau of Reclamation.

Pearse, A.T., Harner, M.J., Baasch, D.M., Wright, G.D., Caven, A.J., Metzger, K.L., 2016. Evaluation of nocturnal roost and diurnal sites used by whooping cranes in the Great Plains, United States. USGS Open-File Report 1209.

Platte River Recover Implementation Program (PRRIP), 2017. Data Synthesis Compilation: Whooping Crane (*Grus americana*) Habitat Synthesis Chapters.

Platte River Recover Implementation Program (PRRIP), 2022. 2022 PRRIP Virtual Science Plan Reporting Session – Independent Scientific Advisory Committee (ISAC) Discussion Questions.

Quantum Spatial Inc. (QSI), 2016. Platte River, Nebraska – Fall 2016: Topobathymetric LiDAR Technical Data Report.

Quantum Spatial Inc. (QSI), 2017. Platte River, Nebraska – Fall 2017: Topobathymetric LiDAR Technical Data Report.

Quantum Spatial Inc. (QSI), 2018. Platte River Fall 2018, Nebraska: Topobathymetric LiDAR Technical Data Report.

Quantum Spatial Inc. (QSI), 2019. Platte River Fall 2019, Nebraska: Topobathymetric LiDAR Technical Data Report.

Quantum Spatial Inc. (QSI), 2020. Platte River Fall 2020, Nebraska: Topobathymetric LiDAR Technical Data Report.

R Core Team, 2017. R: A language and environment for statistical computing. R Foundation for Statistical Computing, Vienna, Austria. URL https://www.R-project.org/.

Rouse, J.W., Haas, R.H., Schell, J.A. & Deering, D.W., 1973. Monitoring vegetation systems in the Great Plains with ERTS. NASA. Goddard Space Flight Center 3d ERTS-1 Symp., Vol. 1, Sect. A

Riverscapes Consortium, 2020. Geomorphic Change Detection. Software and information found at https://github.com/Riverscapes/gcd

Tetra Tech, 2017. 2016 Platte River Final Data Analysis Report: Channel Geomorphology and In-channel Vegetation. Platte River Recovery Implementation Program.

Trimble, 2021. eCognition Version 10.2. https://geospatial.trimble.com/products-and-solutions/ecognition

Wheaton, J.M., Brasington, J., Darby, S.E., Sear, D.A., 2010. Accounting for uncertainty in DEMs from repeat topographic surveys: improved sediment budgets. Earth Surface Processes and Landforms 35.

Wohl, E., Bledsoe, B.P., Jacobson, R.B., Poff, L., Rathburn, S.L., Walters, D.M., Wilcox, A.C., 2015. The natural sediment regime in rivers: broadening the foundation for ecosystem management. BioScience 65.

11. Appendices

A. Revised Draft Monitoring Protocol

- A1. Hydrodynamic Modeling
- A2. Land Cover Classification
- A3. Volume Change

B. Hydrologic Results

C. Hydrodynamic Modeling Results

D. Land Cover Results

E. Volume Change Results